J. Fluid Mech. (2009), *vol.* 639, *pp.* 1–35.
doi:10.1017/S0022112009990620

Buoyancy-dominated displacement flows in near-horizontal channels: the viscous limit

S. M. TAGHAVI[1], T. SEON[2], D. M. MARTINEZ[1] AND I. A. FRIGAARD[2,3]†

[1]Department of Chemical and Biological Engineering, University of British Columbia, 2360 East Mall, Vancouver, BC, Canada V6T 1Z3

[2]Department of Mathematics, University of British Columbia, 1984 Mathematics Road, Vancouver, BC, Canada V6T 1Z2

[3]Department of Mechanical Engineering, University of British Columbia, 6250 Applied Science Lane, Vancouver, BC, Canada V6T 1Z4

(Received 31 December 2008; revised 25 May 2009; accepted 26 May 2009; first published online 16 October 2009)

We consider the viscous limit of a plane channel miscible displacement flow of two generalized Newtonian fluids when buoyancy is significant. The channel is inclined close to horizontal. A lubrication/thin-film approximation is used to simplify the governing equations and a semi-analytical solution is found for the flux functions. We show that there are no steady travelling wave solutions to the interface propagation equation. At short times the diffusive effects of the interface slope are dominant and there is a flow reversal, relative to the mean flow. We are able to find a short-time similarity solution governing this initial counter-current flow. At longer times the solution behaviour can be predicted from the associated hyperbolic problem (where diffusive effects are set to zero). Each solution consists of a number $N \geqslant 1$ of steadily propagating fronts of differing speeds, joined together by segments of interface that are stretched between the fronts. Diffusive effects are always present in the propagating fronts. We explore the effects of viscosity ratio, inclinations and other rheological properties on the front height and front velocity. Depending on the competition of viscosity, buoyancy and other rheological effects, it is possible to have single or multiple fronts. More efficient displacements are generally obtained with a more viscous displacing fluid and modest improvements may also be gained with slight positive inclination in the direction of the density difference. Fluids that are considerably shear-thinning may be displaced at high efficiencies by more viscous fluids. Generally, a yield stress in the displacing fluid increases the displacement efficiency and yield stress in the displaced fluid decreases the displacement efficiency, eventually leading to completely static residual wall layers of displaced fluid. The maximal layer thickness of these static layers can be directly computed from a one-dimensional momentum balance and indicates the thickness of static layer found at long times.

1. Introduction

In this paper we consider miscible displacement flows along a plane channel of width $\hat{D}$ in the large Péclet number limit $Pe \gg 1$ (where $Pe = \hat{D}\hat{U}_0/\hat{D}_m$, with $\hat{U}_0$

† Email address for correspondence: frigaard@mech.ubc.ca

the mean displacement velocity and $\hat{D}_m$ the molecular diffusivity). In this limit, in the absence of any flow instability, the fluids have insufficient time to mix on time scales of experimental interest and a reasonable approximation is to model the two fluids via a kinematic equation, rather than a concentration-diffusion-equation (CDE) approach. The stability of the flow cannot generally be determined beforehand and often the reason for this type of model simplification is to make study of the stability problem possible, as well as to gain basic understanding of the laminar flow. The scenarios that we consider involve fluids of different densities, with Newtonian or non-Newtonian shear rheology.

Within the class of large Péclet number displacement flows, we consider those in which buoyancy is a significant force in driving the fluid motion and restrict our study to those in which the channel is approximately horizontal. In the absence of a mean flow ($\hat{U}_0 = 0$), the only driving force would be buoyancy. For sufficiently small density differences there exists a viscous regime in which inertial effects are small and for which the interface slumps under gravity and elongates along the channel. If now a mean displacement flow is introduced, we may expect that the viscous regime persists for at least small Reynolds numbers Re ($= \hat{\rho}\hat{U}_0\hat{D}/\hat{\mu}$). Indeed, when the flow topology evolves into an elongated slumping interface with near-parallel streamlines, of aspect ratio $\delta \ll 1$, inertial effects remain negligible provided that $\delta Re \ll 1$. This allows for a more practical range of Re to be studied. It is such flows that we consider in this paper.

Although for mathematical simplicity we adopt a plane channel geometry, our motivation comes from duct flows, (commonly pipes). The detailed study of laminar miscible displacement flows in ducts is relatively recent, although of course the dispersive regimes of Taylor (1953) and Aris (1956) were studied much earlier. Many practical processing situations involving aqueous liquids in laminar duct flows with diameters $\hat{D} \sim 10^{-2}$ m and mean velocities $\hat{U}_0 \lesssim 0.1$ m s^{-1} necessarily fall in to the category of high Pe flows, typically in the range 10^3–10^7. However, for such flows the Taylor-dispersion regime is strictly found only for duct lengths $\hat{L} \gg \hat{D}Pe$, which are arguably less common in processing geometries for laminar regimes, even though $\hat{D}/\hat{L} \ll 1$ is usual. Thus, study of the non-dispersive high Pe regime for long ducts has substantial practical application.

This high Pe regime inevitably approaches the zero surface tension immiscible limit ($Pe \to \infty$) provided the displacement flow remains stable, as has been shown analytically, computationally and experimentally in the works of Petitjeans & Maxworthy (1996), Chen & Meiburg (1996), Rakotomalala, Salin & Watzky (1997) and Yang & Yortsos (1997). Briefly, these studies show that sharp interfaces persist over wide ranges of parameters for dimensionless times (hence distances) $t \ll Pe$, with smearing of the interface and effective diffusion across the duct for $t \sim Pe$, eventually approaching the dispersive limit. These studies focus on Newtonian fluids, with little effect of buoyancy. The dispersive limit of miscible isodensity displacements, also for a range of simple non-Newtonian fluids, has been considered by Zhang & Frigaard (2006).

For flows in which buoyancy effects are significant, there is a large literature on gravity currents, stratified flows and mixing in (at least partly) unconfined geometries stemming from oceanographic and environmental applications. Slightly closer to our study are those of lock-exchange flows in tanks (open channels). Such flows are typically studied in a regime where viscous effects are unimportant and buoyancy forces are balanced by inertia. The velocity is essentially constant in each interpenetrating stream. The mathematical approach for studying these flows dates

back to the work of Benjamin (1968) (See Shin, Dalziel & Linden 2004 and references therein for an overview and critical appraisal.). Recently Birman *et al.* (2007) have studied gravity currents in inclined channels. These are high *Re* flows, vulnerable to interfacial instabilities (loosely of Kelvin–Helmholz type), and local mixing. Thus typically the edges of gravity currents are not well defined due to local instability and mixing.

In the absence of an imposed mean flow, a detailed experimental study of buoyancy driven miscible flows in inclined pipes has been carried out by Seon *et al.* (2004, 2005, 2006, 2007). In these studies the pipe is closed at the ends so that an exchange flow results. Seon *et al.* (2005) experimentally characterized the velocity of the interpenetrating fronts of light and heavy fluids, as a function of viscosity ratio, density ratio and inclination angle. For different inclinations of the pipe from horizontal to vertical they observed three flow regimes: increasing front velocity, constant front velocity and decreasing front velocity. In the first regime, found close to horizontal, the fluids are separated into two parallel counter-current streams. In the second regime, the front velocity is independent of inclination angle and fluid viscosity, controlled by the balance between inertia and buoyancy. For the first and the second regimes, they obtained a correlative formulation based on characteristic viscous and inertial velocities. In the last regime segregation and mixing effects control the front velocity.

The near-horizontal regime is studied in more detail by Seon *et al.* (2007), who found a small critical value of inclination, above which the front velocity is fully controlled by inertia. When the inclination is below this critical value, the front velocity is initially controlled by inertia but later by viscosity. As soon as viscous effects start to control the front velocity, it gradually decreases towards a steady-state value, which is proportional to the sine of the inclination angle, from horizontal. This final velocity thus tends to zero for a horizontal tube. They also showed that the fluid concentration/interface profiles depend on the reduced variable $\hat{x}/\sqrt{\hat{t}}$, i.e. spreading diffusively. In viscous regimes for near horizontal pipes the transverse gravitational component suppresses the development of instabilities, so that there is no mixing between the fluids and the interface remains clear. This shift from an initial inertial-buoyancy balance to a viscous-buoyancy balance was also found by Didden & Maxworthy (1982) and Huppert (1982), who considered viscous spreading of gravity currents with an imposed flow. In the absence of an imposed mean flow there is some subtlety in the transition between strictly horizontal ducts and slightly inclined ducts. Buoyancy acts both via the slope of the duct and the slope of the interface, relative to the duct axis. When the interface elongates the latter effect of buoyancy diminishes but the former effect remains present. For our study there is a third driving force, that of the imposed flow, which does not diminish over time. Thus, the distinction between strictly horizontal ducts and slightly inclined ducts is not so critical as in the analysis in Seon *et al.* (2007).

Also related to our study are studies of viscous spreading of thin layers fed with an imposed flow at a source. These arise in particular in the context of lava dome formation and spreading (see Griffiths 2000). Frequently, the models and experiments used to understand these phenomena are complicated with thermal effects, which then bears little resemblance to our work. However, Balmforth *et al.* (2000) and Balmforth, Craster & Sassi (2002) have studied lava dome formation in an isothermal setting and with viscoplastic fluids of the type considered here. Although the lubrication/thin-film modelling is similar, these flows are unconstrained single fluid flows in which the flux function is typically determined analytically and hence progress is simpler.

The literature for non-Newtonian fluid displacements in ducts is obviously less developed than that for Newtonian displacements. By far the largest body of work concerns Hele-Shaw geometries, where there are several numerical, experimental and analytical studies of viscous fingering with non-Newtonian fluids; see Wilson (1990), Sader, Chan & Hughes (1994), Kondic, Palffy-Muhoray & Shelley (1996), Coussot (1999) and Lindner, Coussot & Bonn (2000) as examples. Gas–liquid displacements in tubes have been studied for viscoplastic fluids by Dimakopoulos & Tsamopoulos (2003, 2007) and by De Sousa *et al.* (2007). The focus here is typically on residual layers in steady-state displacements. The flow around the displacement front is multi-dimensional. Other multi-dimensional displacement flows with generalized Newtonian fluids have been studied, numerically and analytically by Allouche, Frigaard & Sona (2000) and Frigaard, Scherzer & Sona (2001), as well as experimentally by Gabard (2001) and Gabard & Hulin (2003). These are all isodensity viscous-dominated displacements of miscible fluids in the high *Pe* regime.

In such viscous-dominated flows various instabilities arise. Interfacial instabilities of 'bamboo' type were reported by Joseph & Renardy (1993) in the context of oil–water parallel flows. Similar instabilities have been observed by Gabard (2001) and by Gabard & Hulin (2003) in their displacement flow studies, also when the interface elongates and the flow is pseudo-parallel. The viscosity ratio in Gabard's studies is inverse to that reported in Joseph & Renardy (1993) and the instabilities are instead of 'inverted bamboo' type. Frontal instabilities were evidenced in a sequence of miscible displacement studies by Lajeunesse and coworkers. Lajeunesse *et al.* (1997, 1999) investigated the downward vertical miscible displacement of fluids in the gap of a Hele-Shaw cell at high velocities. They distinguished a base two-dimensional state in which a tongue of constant thickness propagates steadily. For certain viscosity ratios and flow rates the two-dimensional pattern breaks into three-dimensional fingers. These are studied in more detail in Lajeunesse *et al.* (2001). Of more interest to our study is the observation of critical viscosity ratios at which the steady front shows shock-like behaviour and other viscosity ratios for which the propagation of multiple fronts at different speeds is observed, including a rapidly moving 'spike' in the channel centre. A lubrication-type displacement model is advanced to explain these non-inertial phenomena.

Motivation for our study comes from various operations present in the construction and completion of oil wells (e.g. primary cementing, see Nelson 1990, drilling, gravel packing, fracturing). These processes often involve displacing one fluid with another or with a sequence of different fluids. The geometries are typically pipe, annular or duct-like, all with long aspect ratios. Large volumes are pumped so that fluids may be considered separated, i.e. we have a two-fluid displacement, not an n-fluid displacement. A very wide range of fluids are used. Density differences of up to 500 kg m^{-3} can occur, shear-thinning and yield stress rheological behaviours are widely found and are often the dominant non-Newtonian effects, (more exotic non-Newtonian effects may also be present). Our study is part of a wider effort to understand these flows in some generality, using experimental, numerical and analytical methodologies. Here we focus on a limiting parameter regime that appears to be tractable (semi-) analytically and which also has practical relevance.

In terms of what may be expected, more efficient displacements are generally found with more viscous displacing fluids. Thus, in dealing with non-Newtonian fluids we may expect some generalization of this effect. Part of the task is to quantify this notion of 'more viscous' in terms of the displacement. For example, with shear-thinning fluids we may have fluid pairs for which one fluid is more/less viscous than

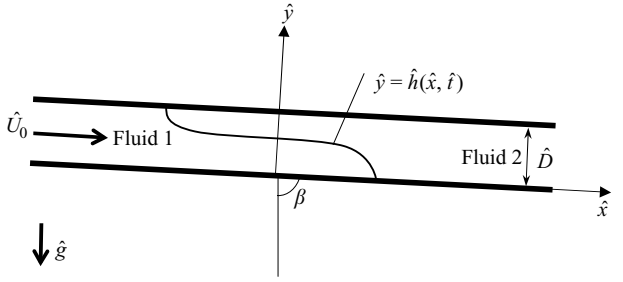

FIGURE 1. Schematic of displacement geometry.

the other at high/low shear rates or vice versa. In the case of yield stress fluids, it is known that displacements may lead to static wall layers, as studied in Allouche *et al.* (2000). Unlike purely viscous non-Newtonian fluids, the displacement efficiency can asymptote to a value less than 1, and identification of this regime is consequently important. On the other hand, inclusion of a yield stress in the displacing fluid has the general effect of increasing viscosity.

An outline of the paper is as follows. Section 2 discusses the geometry of the problem, derives simplified model equations and, in § 2.4, we show analytically that there are no steady-state displacement solutions to this problem. In § 3, we present an analysis of both long- and short-time model behaviours, for Newtonian displacement flows. Shear-thinning and yield stress effects are considered in § 4. The paper closes with a brief discussion and summary in § 5.

2. Two-fluid displacement flows in a near-horizontal slot

We consider a two-dimensional region between two parallel plates, separated by a distance $\hat{D}$, that are oriented at an angle $\beta \approx \pi/2$ to the vertical. The slot is initially filled with fluid 2, which is displaced by fluid 1, injected at $\hat{x} = -\infty$ with a mean velocity $\hat{U}_0$. Cartesian coordinates $(\hat{x}, \hat{y})$ are as shown in figure 1. Both fluids are assumed to be generalized Newtonian fluids, with rheologies described below, and although the fluids are miscible we consider the large Péclet number limit in which no significant mixing occurs over the time scales of interest. The dimensionless equations of motion, valid within each fluid region Ω_k, $k = 1, 2$, are

$$\phi_k Re \left[\frac{\partial u}{\partial t} + u \frac{\partial u}{\partial x} + v \frac{\partial u}{\partial y} \right] = -\frac{\partial p}{\partial x} + \frac{\partial}{\partial x} \tau_{k,xx} + \frac{\partial}{\partial y} \tau_{k,xy} + \phi_k \frac{\cos \beta}{St}, \tag{2.1}$$

$$\phi_k Re \left[\frac{\partial v}{\partial t} + u \frac{\partial v}{\partial x} + v \frac{\partial v}{\partial y} \right] = -\frac{\partial p}{\partial y} + \frac{\partial}{\partial x} \tau_{k,yx} + \frac{\partial}{\partial y} \tau_{k,yy} - \phi_k \frac{\sin \beta}{St}, \tag{2.2}$$

$$\frac{\partial u}{\partial x} + \frac{\partial v}{\partial y} = 0. \tag{2.3}$$

Here $\boldsymbol{u} = (u, v)$ denotes the velocity, p the pressure and $\tau_{k,ij}$ is the ijth component of the deviatoric stress in fluid k. The parameter $\phi_1 \equiv 1$, and the three dimensionless parameters appearing above are the density ratio ϕ_2, the Reynolds number Re and the Stokes number St defined as follows:

$$\phi_2 = \phi \equiv \frac{\hat{\rho}_2}{\hat{\rho}_1}, \quad Re \equiv \frac{\hat{\rho}_1 \hat{U}_0 \hat{D}}{\hat{\mu}_1}, \quad St \equiv \frac{\hat{\mu}_1 \hat{U}_0}{\hat{\rho}_1 \hat{g} \hat{D}^2}. \tag{2.4}$$

Here $\hat{\rho}_k$ is the density of fluid k, $\hat{\mu}_1$ is a viscosity scale for fluid 1 and $\hat{g}$ is the gravitational acceleration. Further dimensionless parameters will appear in constitutive laws, defining the deviatoric stresses. In order to derive (2.1)–(2.3) we have scaled distances using $\hat{D}$, velocities with $\hat{U}_0$, time with $\hat{D}/\hat{U}_0$, pressure and stresses with $\hat{\mu}_1\hat{U}_0/\hat{D}$.

On the walls of the slot the no-slip condition is satisfied. Due to the scaling adopted, we have

$$\int_0^1 u \, \mathrm{d}y = 1, \tag{2.5}$$

in each cross-section. The slot is assumed infinite in x, with the interface between fluids initially localized close to $x = 0$. We shall consider flows that are buoyancy dominated, in which the heavier fluid lies at the bottom of the slot, separated from the lighter upper fluid by an interface that we denote by $y = h(x, t)$ and assume to be single valued. Across the interface, velocity and stress are continuous. The interface is simply advected with the flow, satisfying a kinematic condition.

2.1. *Constitutive laws*

The fluids are assumed to be generalized Newtonian fluids. In particular we are interested to understand shear thinning and yield stress effects. A suitable model that incorporates these effects is the Herschel–Bulkley model, which incorporates also the simpler Bingham, power law and Newtonian models. Constitutive laws for the Herschel–Bulkley fluids are

$$\dot{\gamma}(\boldsymbol{u}) = 0 \iff \tau_k(\boldsymbol{u}) \leqslant B_k, \qquad \boldsymbol{x} \in \Omega_k, \tag{2.6}$$

$$\tau_{k,ij}(\boldsymbol{u}) = \left[\kappa_k \dot{\gamma}^{n_k - 1}(\boldsymbol{u}) + \frac{B_k}{\dot{\gamma}(\boldsymbol{u})}\right] \dot{\gamma}_{ij}(\boldsymbol{u}) \iff \tau_k(\boldsymbol{u}) > B_k, \qquad \boldsymbol{x} \in \Omega_k, \tag{2.7}$$

where the strain rate tensor has components

$$\dot{\gamma}_{ij}(\boldsymbol{u}) = \frac{\partial u_i}{\partial x_j} + \frac{\partial u_j}{\partial x_i}, \tag{2.8}$$

and the second invariants $\dot{\gamma}(\boldsymbol{u})$ and $\tau_k(\boldsymbol{u})$ are defined by

$$\dot{\gamma}(\boldsymbol{u}) = \left[\frac{1}{2}\sum_{i,j=1}^{2} [\dot{\gamma}_{ij}(\boldsymbol{u})]^2\right]^{1/2}, \quad \tau_k(\boldsymbol{u}) = \left[\frac{1}{2}\sum_{i,j=1}^{2} [\tau_{k,ij}(\boldsymbol{u})]^2\right]^{1/2}. \tag{2.9}$$

Herschel–Bulkley fluids are described by three-dimensional parameters: a fluid consistency $\hat{\kappa}$, a yield stress $\hat{\tau}_Y$ and a power law index n. The parameter $\kappa_1 = 1$ and κ_2 is the viscosity ratio m:

$$m \equiv \frac{\hat{\mu}_2}{\hat{\mu}_1} = \frac{\hat{\kappa}_2[\hat{U}_0/\hat{D}]^{n_2 - 1}}{\hat{\kappa}_1[\hat{U}_0/\hat{D}]^{n_1 - 1}}, \tag{2.10}$$

where $\hat{\mu}_2$ is a viscosity scale for fluid 2. Note that in the case of two Newtonian fluids, $\hat{\mu}_k = \hat{\kappa}_k$. The Bingham numbers B_k are defined as

$$B_k \equiv \frac{\hat{\tau}_{k,Y}}{\hat{\kappa}_1[\hat{U}_0/\hat{D}]^{n_1}}. \tag{2.11}$$

2.2. *Buoyancy dominated flows:* $|\phi - 1|/St \gg 1$

The objective of our study is to understand a particular limit of (2.1)–(2.3), in which inertia is not considered to be dominant and the interface orients approximately

horizontally along the axis of the slot: moderate Re, $\beta \approx \pi/2$ and $\phi \sim O(1)$. The ratio of buoyancy to viscous forces is given by the parameter $|\phi - 1|/St$. We suppose that $|\phi - 1|/St \gg 1$ so that the interface elongates over some (dimensionless) length scale $\delta^{-1} \gg 1$. To define this length scale we assume that the dynamics of spreading of the interface, relative to the mean flow, will be driven by buoyant stresses which have size: $|\hat{\rho}_1 - \hat{\rho}_2|\hat{g} \sin\beta \hat{D}$ in the y direction. These stresses, which act across the interface where there is a density difference, translate into axial stresses according to the slope of the interface. If the slope of the interface has size $\hat{D}/\hat{L}$, the stress that acts to spread the flow axially has size $|\phi - 1|\hat{\rho}_1 \hat{g} \sin\beta \hat{D}^2/\hat{L}$. This tendency to spread is resisted by viscous stresses within the fluids, of size $\hat{\mu}_1 \hat{U}_0/\hat{D}$, which dissipate the energy injected by buoyancy. By matching these two terms, we can obtain the characteristic spreading length in this regime:

$$|\phi - 1|\hat{\rho}_1 \hat{g} \sin\beta \hat{D}^2/\hat{L} = \hat{\mu}_1 \hat{U}_0/\hat{D} \Rightarrow \hat{L} = \frac{|\phi - 1|\hat{\rho}_1 \hat{g} \sin\beta \hat{D}^3}{\hat{\mu}_1 \hat{U}_0}. \tag{2.12}$$

Thus, the ratio between the axial length scale and channel width is

$$\delta^{-1} = \frac{\hat{L}}{\hat{D}} = \frac{|\phi - 1|\hat{\rho}_1 \hat{g} \sin\beta \hat{D}^2}{\hat{\mu}_1 \hat{U}_0} = \frac{|\phi - 1| \sin\beta}{St}. \tag{2.13}$$

Following standard methods (see, e.g. Leal 2007) we rescale as follows:

$$\delta x = \xi, \quad \delta t = T, \quad \delta p = P, \quad v = \delta V,$$

and arrive at the following reduced system of equations, in each fluid region Ω_k, $k = 1, 2$:

$$\delta \phi_k Re \left[\frac{\partial u}{\partial T} + u\frac{\partial u}{\partial \xi} + V\frac{\partial u}{\partial y}\right] = -\frac{\partial P}{\partial \xi} + \frac{\partial}{\partial y}\tau_{k,\xi y} + \phi_k \frac{\cos\beta}{St} + O(\delta^2),$$

$$\delta^3 \phi_k Re \left[\frac{\partial V}{\partial T} + u\frac{\partial V}{\partial \xi} + V\frac{\partial V}{\partial y}\right] = -\frac{\partial P}{\partial y} - \delta \phi_k \frac{\sin\beta}{St} + O(\delta^2),$$

$$\frac{\partial u}{\partial \xi} + \frac{\partial V}{\partial y} = 0.$$

To aid interpretation of our model results, note that the time and length variables (T, ξ) are related to the dimensional time and length by

$$\frac{|\hat{\rho}_1 - \hat{\rho}_2|\hat{g} \sin\beta \hat{D}^3}{\hat{\mu}_1 \hat{U}_0}\xi = \hat{x}, \quad \frac{|\hat{\rho}_1 - \hat{\rho}_2|\hat{g} \sin\beta \hat{D}^3}{\hat{\mu}_1 \hat{U}_0^2}T = \hat{t}. \tag{2.14}$$

Note that we have used $\hat{D}/\hat{U}_0$ to scale $\hat{t}$, which is the usual convective time scale based on the mean velocity and $\hat{D}$. Therefore, the scale related to the *slow time* variable T corresponds to the time taken to travel the characteristic spreading length $\hat{L}$ at mean velocity $\hat{U}_0$.

We now consider the limit $\delta \to 0$ with Re fixed:

$$0 = -\frac{\partial P}{\partial \xi} + \frac{\partial}{\partial y}\tau_{k,\xi y} + \chi \frac{\phi_k}{|1 - \phi|}, \tag{2.15}$$

$$0 = -\frac{\partial P}{\partial y} - \frac{\phi_k}{|1 - \phi|}, \tag{2.16}$$

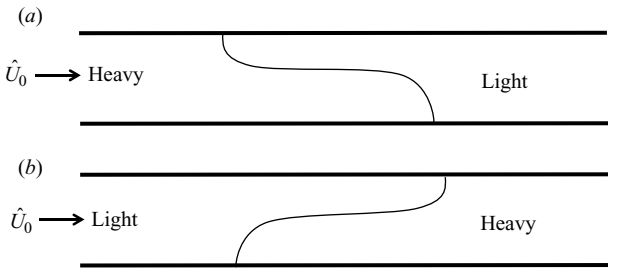

FIGURE 2. Schematic of displacement types considered: (*a*) heavy fluid displaces light fluid (HL displacement); (*b*) light fluid displaces heavy fluid (LH displacement).

where $\chi = \cot\beta/\delta$. The parameter χ measures the relative importance of the slope of the channel to the slope of the interface, in driving buoyancy related motions. We wish to consider channels that are close to horizontal, where the slopes of both the channel and the interface may be of comparable importance. Thus, we assume χ is an order 1 parameter, i.e. we consider inclinations $\beta = \pi/2 + O(\delta)$. For $\chi > 0$ the slope of the channel is 'downhill', in the direction of the flow, and for $\chi < 0$ the flow is uphill. Note that for larger χ the model does not necessarily break down, but effectively we have chosen the wrong scaling as the effect of the channel slope is dominant.

Before proceeding, we observe that there are two qualitatively different types of displacement flows:

(*a*) HL (heavy–light) displacement: fluid 1 is heavier than fluid 2, and the lower layer of fluid is consequently fluid 1. Parameters are $(n_H, \kappa_H, B_H, n_L, \kappa_L, B_L) = (n_1, 1, B_1, n_2, m, B_2)$.

(*b*) LH (light–heavy) displacement: fluid 1 is lighter than fluid 2, and the lower layer of fluid is consequently fluid 2. Parameters are $(n_H, \kappa_H, B_H, n_L, \kappa_L, B_L) = (n_2, m, B_2, n_1, 1, B_1)$.

These are illustrated schematically in figure 2. We do not consider mechanically unstable configurations, i.e. heavy fluid over light fluid.

We integrate (2.16) across both fluid layers to give the pressure:

$$P(\xi, y, T) = \begin{cases} P_0(\xi, T) + \chi \dfrac{\phi_H}{|1-\phi|}\xi - \dfrac{\phi_H}{|1-\phi|}y & y \in [0, h], \\ P_0(\xi, T) + \chi \dfrac{\phi_H}{|1-\phi|}\xi - \dfrac{\phi_H - \phi_L}{|1-\phi|}h - \dfrac{\phi_L}{|1-\phi|}y & y \in [h, 1], \end{cases} \tag{2.17}$$

where $P_0(\xi, T)$ is defined by

$$P_0(\xi, T) = P(\xi, 0, T) - \chi \frac{\phi_H}{|1-\phi|}\xi,$$

with $\phi_H = \hat{\rho}_H/\hat{\rho}_1$ for the heavier fluid, $\phi_L = \hat{\rho}_L/\hat{\rho}_1$ for the lighter fluid. On substituting into (2.15), we arrive at

$$0 = -\frac{\partial P_0}{\partial \xi} + \frac{\partial}{\partial y}\tau_{H,\xi y}, \quad y \in (0, h), \tag{2.18}$$

$$0 = -\frac{\partial P_0}{\partial \xi} + \frac{\partial}{\partial y}\tau_{L,\xi y} - \chi + \frac{\partial h}{\partial \xi}, \quad y \in (h, 1). \tag{2.19}$$

In the lubrication approximation, the leading order strain rate component is $\dot{\gamma}_{\xi y} = \partial u/\partial y$, and the leading order shear stress $\tau_{k,\xi y}$ is defined in terms of $\dot{\gamma}_{\xi y}$ via the

following leading order constitutive laws:

$$\frac{\partial u}{\partial y} = 0 \Longleftrightarrow |\tau_{k,\xi y}| \leqslant B_k, \qquad \boldsymbol{x} \in \Omega_k, \tag{2.20}$$

$$\tau_{k,\xi y} = \left[\kappa_k \left| \frac{\partial u}{\partial y} \right|^{n_k - 1} + \frac{B_k}{\left| \dfrac{\partial u}{\partial y} \right|} \right] \frac{\partial u}{\partial y} \Longleftrightarrow |\tau_{k,\xi y}| > B_k, \qquad \boldsymbol{x} \in \Omega_k. \tag{2.21}$$

Thus, for given h and $\partial h/\partial \xi$, (2.18) and (2.19) define an elliptic problem for $u(y)$. Boundary conditions for $u(y)$ are $u = 0$ at $y = 0, 1$. At the interface, $y = h$, u is continuous and $\tau_{H,\xi y} = \tau_{L,\xi y}$, representing stress continuity. These four conditions are sufficient to determine u for given $\partial P_0/\partial \xi$. The pressure gradient is determined by the additional constraint that (2.5) is satisfied.

For now we assume that the solution of this problem may be computed and we note that the dependence of u on (ξ, T) enters only via $h(\xi, T)$, which satisfies

$$\frac{\partial h}{\partial T} + u \frac{\partial h}{\partial \xi} = V. \tag{2.22}$$

Combining the kinematic equation with the divergence free constraint leads, in the usual manner, to the equation

$$\frac{\partial h}{\partial T} + \frac{\partial}{\partial \xi} q(h, h_\xi) = 0, \tag{2.23}$$

where $q(h, h_\xi)$ is defined as

$$q(h, h_\xi) = \int_0^h u(y, h, h_\xi)\, \mathrm{d}y. \tag{2.24}$$

The remainder of our study concerns behaviour of solutions to the system (2.23) and (2.24).

As boundary conditions, for an HL displacement we have that

$$h(\xi, T) \to 1, \text{ as } \xi \to -\infty; \quad h(\xi, T) \to 0, \text{ as } \xi \to \infty, \tag{2.25}$$

as the channel is assumed full of pure fluid 1 and fluid 2 at the two ends of the channel. As initial conditions we note that an initial profile in the unscaled variables $h(x, t = 0) = h_0(x)$ is transformed to $h(\xi, T = 0) = h_0(\xi/\delta)$. Since h_0 should be compatible with the far-field conditions we have that as $\delta \to 0$,

$$h(\xi, 0) \to 1 - H(\xi), \tag{2.26}$$

where $H(\xi)$ is the usual Heaviside function. In other words, in terms of ξ, the initial change in h is localized to $\xi = 0$. For an LH displacement this is reversed, i.e.

$$h(\xi, T) \to 0, \text{ as } \xi \to -\infty; \quad h(\xi, T) \to 1, \text{ as } \xi \to \infty, \tag{2.27}$$

$$h(\xi, 0) = H(\xi), \tag{2.28}$$

since the far-field pure fluids are reversed.

2.3. *The flux function* $q(h, h_\xi)$

In the general case, finding the flux function $q(h, h_\xi)$ requires computation, and this is addressed in Appendix A. For the particular case of a Newtonian fluid the analytical

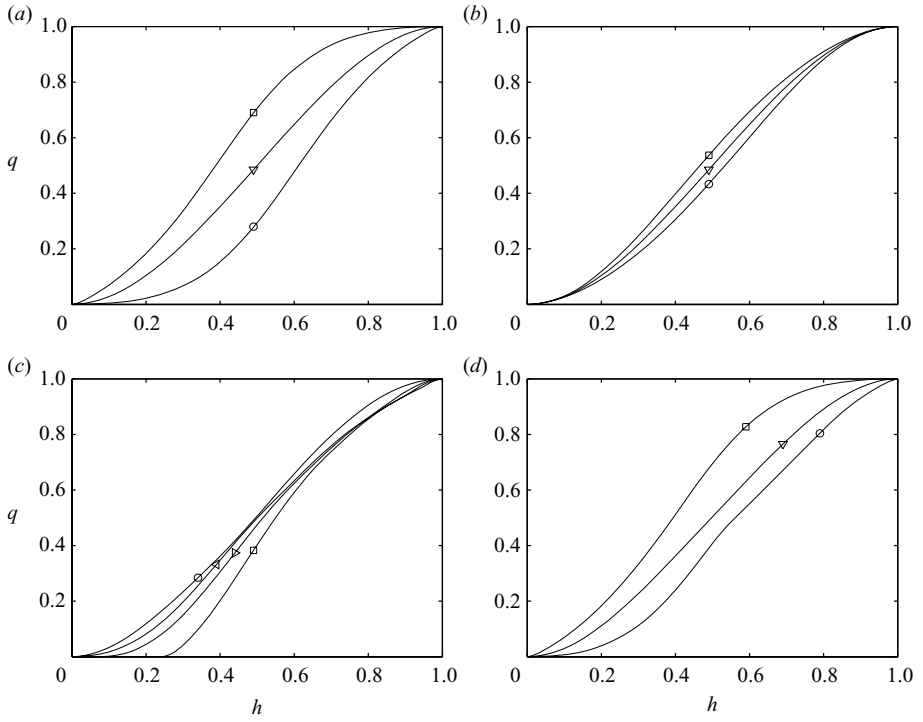

FIGURE 3. Examples of q for two Newtonian fluids: (a) $b=0$ and different m; HL displacement with $m=0.1$ ($\bigcirc$), $m=1$ ($\triangledown$), $m=10$ ($\square$); LH displacement with $m=10$ ($\bigcirc$), $m=1$ ($\triangledown$), $m=0.1$ ($\square$); (b) $m=1$ and different b; HL or LH displacements with $b=-10$ ($\bigcirc$), $b=0$ ($\triangledown$), $b=10$ ($\square$). Examples of q for two non-Newtonian fluids in HL displacement: (c) $b=1$, $m=1$, $B_2=1$, $n_k=1$, $B_1=0$ ($\bigcirc$), $B_1=5$ ($\triangleleft$), $B_1=10$ ($\triangleright$), $B_1=20$ ($\square$); (d) $b=1$, $B_k=1$, $n_k=1$, $m=0.1$ ($\bigcirc$), $m=1$ ($\triangledown$), $m=10$ ($\square$).

solution may be found trivially. Denoting $b=\chi-h_\xi$, for an HL displacement we find

$$q(h;b,m) \;=\; q_A(h;m)+bq_B(h;m). \tag{2.29}$$

where $q_A(h;m)$ and $q_B(h;m)$ represent the advective and buoyancy-driven components of the flux $q(h;b,m)$:

$$q_A(h;m) \;=\; \frac{3mh^2(mh^2+(h+3)(1-h))}{3[(1-h)^4+2mh(1-h)(h^2-h+2)+m^2h^4]}, \tag{2.30}$$

$$q_B(h;m) \;=\; \frac{[h^3(1-h)^3(mh+(1-h))]}{3[(1-h)^4+2mh(1-h)(h^2-h+2)+m^2h^4]}. \tag{2.31}$$

For an LH displacement, the flux function is given by

$$q(h;b,m) \;=\; q_A(h;1/m)+bq_B(h;1/m). \tag{2.32}$$

Examples of computed q are given in figure 3. For all examples, these functions have been computed using the procedure described in Appendix A, with the results compared against (2.29) in the case of Newtonian fluids, to verify the numerical method.

We observe that the curves for $m=0.1$ and $m=10$ in figure 3(a), (with $b=0$), show a reflective symmetry, as do those for $b=\pm 10$ in figure 3(b), (with $m=1$). Note also that in figures 3(a) and 3(b), the flux functions are relevant to both HL and LH

displacements, but with m replaced by $1/m$ in the case of LH displacements. This apparent symmetry between HL and LH displacements is not obvious. Note that although the fluxes are mathematically identical for the same b, in fact $b=\chi-h_\xi$ will not be the same since h_ξ will have different sign between the two displacement types. In addition, m is the ratio of displaced to displacing fluid viscosity, which changes with the displacement type. In other words, replacing m with $1/m$ and switching from HL to LH does give the same q, but does not give the same 'shape' of interface (meaning that we replace h with $1-h$, since the LH displacement front slumps along the top of the channel). Instead the HL and LH interfaces are the same shape for the same m in the case of a horizontal channel $\chi=0$, (see figures 4*c* and 4*d*), and will be the same shape for small inclinations if we retain the same m and replace χ with $-\chi$. This does not therefore contradict observations from lubrication-type models of isodensity displacements with central finger-like interfaces, where the cases m and $1/m$ also produce markedly different results.

Figures 3(*c*) and 3(*d*) illustrate non-Newtonian effects on q in HL displacements. In figure 3(*c*) we observe that as the heavy fluid yield stress B_1 is increased $q=0$ in some interval of small h. For these thin layers the yield stress fluid remains static. In figure 3(*d*) we see that the effects of viscosity ratio m is broadly similar for non-Newtonian and Newtonian fluids. For the examples shown, q increases monotonically with little apparent effect of varying the parameters. This is however not always the case, as we have presented only a limited subset of the six parameters, mostly of $O(1)$. With more slightly extreme parameter combinations it is not difficult to find q that are non-monotone, for example. We shall see later that most of the qualitative information concerning the long-term behaviour of the solution is contained in $\partial q/\partial h$, for which the differences are significant.

2.4. *The existence of steady travelling wave displacements.*

One of the most important practical questions in considering this displacement flow is whether or not (2.23) and (2.24) admit steady travelling wave solutions. This determines whether or not the displacement can be effective. In this section we demonstrate that, regardless of fluid type and of rheological differences between fluids, it is impossible for there to be a steady travelling wave solution. Having discounted this possibility, in later sections we turn to a qualitative description of the solutions for different fluid types.

First, let us note that the slope of the interface h_ξ acts always to spread the interface. To see this note that following the construction of the previous section, we may write $q(h,h_\xi)=q(h,b)$ where $b=\chi-h_\xi$. Formally we may write (2.23) as

$$\frac{\partial h}{\partial T}+\frac{\partial q}{\partial h}\frac{\partial h}{\partial \xi}=-\frac{\partial q}{\partial b}\frac{\partial b}{\partial \xi}=\frac{\partial q}{\partial b}\frac{\partial^2 h}{\partial \xi^2}, \tag{2.33}$$

from which we see that the interface spreads diffusively provided that $q(h,b)$ increases with b. We prove the following result in Appendix B.

LEMMA 1. *$q(h,b)$ is non-decreasing for all b.*

Now we examine the condition for there to be a steady travelling wave solution. Since fluid 1 is injected at mean speed 1, the only steady speed that needs be considered is unity. Shifting to a moving frame of reference, say $z=\xi-T$, we see that if the solution is steady in this frame $h=h(z)$, we must have that

$$\frac{\mathrm{d}}{\mathrm{d}z}\left[h-q\left(h,\chi-\frac{\mathrm{d}h}{\mathrm{d}z}\right)\right]=0,$$

and since $q=0$ at $h=0$, this implies that

$$h = q\left(h, \chi - \frac{\mathrm{d}h}{\mathrm{d}z}\right), \tag{2.34}$$

must be satisfied for all $h \in [0, 1]$ if there is to be a steady travelling wave solution. For an HL displacement we impose the further conditions that $h(z)$ decreases monotonically from 1 to 0 with z. For an LH displacement these conditions are reversed: $h(z)$ increases monotonically from 0 to 1 with z. Using Lemma 1, with $b = \chi - \mathrm{d}h/\mathrm{d}z$ we see that the following is true.

LEMMA 2. *For an HL displacement, a necessary condition for there to be steady travelling wave solution is that $q(h, \chi) \leqslant h$ for all $h \in [0, 1]$. For an LH displacement, a necessary condition for there to be steady travelling wave solution is that $q(h, \chi) \geqslant h$ for all $h \in [0, 1]$.*

This follows directly since for an HL displacement we require that $\mathrm{d}h/\mathrm{d}z \leqslant 0$ so that $q(h, b) \geqslant q(h, \chi)$. If this condition is not satisfied we would therefore be unable to find a solution to (2.34), similarly for the LH displacement. Following the procedures in Carrasco-Teja *et al.* (2008) we can in fact show that the conditions of Lemma 2 are in fact sufficient as well as necessary.

Finally, we shall show that the conditions of Lemma 2 are in fact never satisfied. We focus only on the HL displacement, the LH displacement being treated similarly. We consider solutions $u(y)$ to the system

$$\frac{\partial}{\partial y}\tau_{H,\xi y} = -f, \quad y \in (0, h),$$

$$\frac{\partial}{\partial y}\tau_{L,\xi y} = \chi - f, \quad y \in (h, 1),$$

for any of the constitutive laws, with no slip at the walls and continuity of stress and velocity at $y=h$, plus the flow rate constraint (2.5), which determines f. We fix χ and consider $h = 1-\epsilon$, noting first that both the velocity solution and $f(h)$ will vary smoothly with h. For any $h \in [0, 1]$ we note that the shear stress throughout the light fluid layer is given by

$$\tau_{L,\xi y}(y; h) = \tau_{L,\xi y}(1; h) + (1-y)(f(h) - \chi),$$

and as $h \to 1$, we have

$$\tau_{L,\xi y}(y; h) \sim \tau_{L,\xi y}(1; 1) - \epsilon\frac{\partial \tau_{L,\xi y}}{\partial h}(1; 1) + \epsilon(f(1) - \chi) + O(\epsilon^2).$$

Thus, the velocity gradient within the light fluid layer is given by

$$\frac{\partial u}{\partial y} = \frac{\partial u}{\partial y}(\tau_{L,\xi y}(1; 1)) + O(\epsilon),$$

where the algebraic relation for the velocity gradient comes directly from the constitutive laws. Hence we may straightforwardly compute the flux in the lighter fluid layer:

$$q_L(\epsilon) = \int_h^1 u(y)\mathrm{d}y \sim -\frac{\epsilon^2}{2}\frac{\partial u}{\partial y}(\tau_{L,\xi y}(1; 1)) + O(\epsilon^3).$$

Now when $h=1$ the channel is full with the heavy fluid, and the pressure gradient corresponds to the Poiseuille flow solution, say $f(1) = f_H(1) > 0$, which can be easily

calculated. The stress at the upper wall is thus $-0.5f_H(1)$ and since the shear stress is continuous we have

$$\tau_{L,\xi y}(1;1) = -0.5f_H(1) < 0 \quad \Rightarrow \quad q_L(\epsilon) \sim -\frac{\epsilon^2}{2}\frac{\partial u}{\partial y}(-0.5f_H(1)) > 0.$$

Since via the flow rate constraint we have that the total flux is equal to unity, we have that

$$q(h, \chi) \sim 1 + \frac{(1-h)^2}{2}\frac{\partial u}{\partial y}(-0.5f_H(1)) > h, \text{ as } h \to 1. \tag{2.35}$$

Consequently for an HL displacement the necessary conditions of Lemma 2 are always violated sufficiently close to $h = 1$, regardless of fluid type and rheological differences. Similarly, we can show that for an LH displacement the necessary conditions of Lemma 2 are always violated sufficiently close to $h = 0$, regardless of fluid type and rheological differences. This leads to the following result.

LEMMA 3. *There are no steady travelling wave solutions to (2.23).*

Remarks:

(i) This is the key theoretical result of the paper. It is perhaps surprising that for no combination of rheology or density differences are we able to achieve a 'perfect' displacement, (under the assumptions of the lubrication displacement model). This changes the focus of the study. First, in order to achieve a good displacement, we are driven to study those parameter combinations that give the best efficiency, close to 100 %. Second, if we wish to improve the efficiency we need consider phenomena that might do this, other than those accounted for in this simplistic model, e.g. hydrodynamic instability and mixing, or the short-time dynamics in the interfacial region before the interface slumps.

(ii) For a Newtonian fluid displacement, we might find this result rather more directly as the solution may be computed. For example, in Seon *et al.* (2007) the simpler problem of two Newtonian fluids of identical viscosity in an inclined pipe is considered, in the absence of a mean imposed flow. No travelling wave solutions are found. Here, however, the mean flow results in a different structure to the flux functions q, i.e. for Newtonian fluids the advective and buoyant components q_A and q_B are present whereas only q_B is present in Seon *et al.* (2007), (also with an algebraically different form). For non-Newtonian fluids the division of the flux into q_A and q_B is not possible, due to nonlinearity. Thus, we have to work with qualitative properties of the fluxes for such fluids. While we might anticipate from results such as Seon *et al.* (2007) that no travelling waves solutions to (2.23) can be found, from a physical perspective addition of a constant volume flux (i.e. a displacement) makes this a natural and legitimate question.

(iii) Although we have focused on Herschel–Bulkley fluids for definiteness, the same results could be demonstrated for any of the popular generalized Newtonian models, e.g. Carreau fluids, Cross model, Casson model, etc.

3. Newtonian fluids

We commence with an analysis of Newtonian fluid displacements. Although the industrial applications discussed in § 1 typically involve non-Newtonian fluids, many of the qualitative behaviours are exhibited in a Newtonian fluid displacement. Analysis of the Newtonian fluid case not only provides simplification in terms of the number

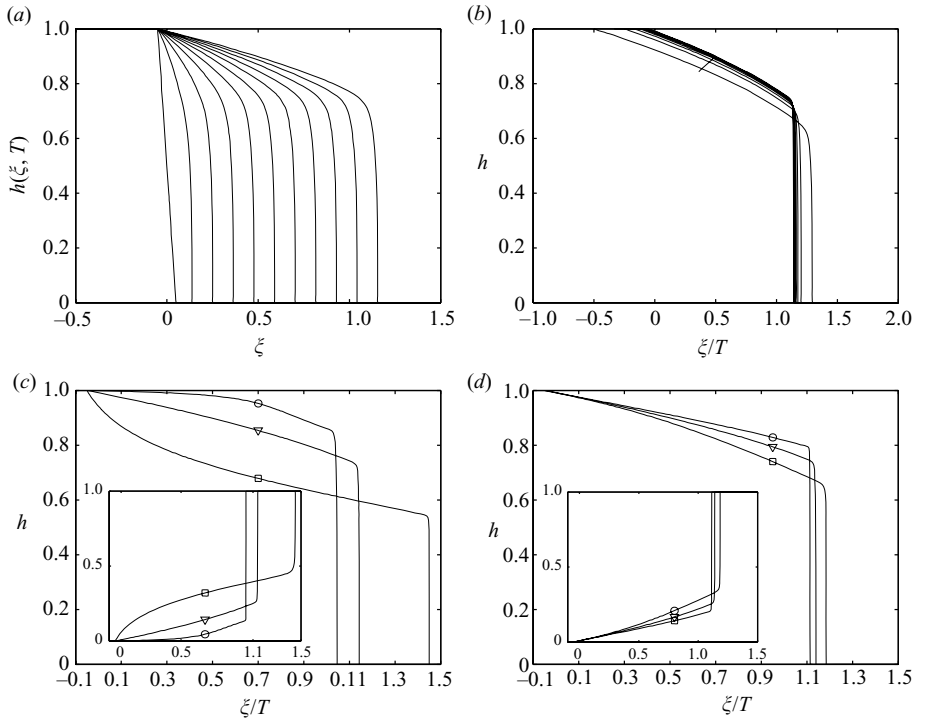

FIGURE 4. Examples of HL displacements: (*a*) $h(\xi, T)$ for $T = 0, 0.1, \ldots, 0.9, 1$, parameters $\chi = 0$, $m = 1$; (*b*) $h(\xi/T)$ for $T = 1, \ldots, 9, 10$, parameters $\chi = 0$, $m = 1$. Examples of HL displacements: (*c*) $h(\xi/T)$ for $\chi = 0$: $m = 0.1$ (○), $m = 1$ (▽), $m = 10$ (□); (*d*) $h(\xi/T)$ for $m = 1$: $\chi = -10$ (○), $\chi = 0$ (▽), $\chi = 10$ (□). The inset figures in (*c*) and (*d*) show the results of LH displacements for the same parameters.

of dimensionless parameters, i.e. (m, χ), but also since q is given by the analytical expression (2.29) numerical solution is considerably faster. For non-Newtonian fluids, each evaluation of q requires numerical solution of the nested iteration described in § A.

The convection–diffusion equation (2.23) was discretized in the conservative form, second order in space and first order in time; and afterward, integrated straightforwardly by using a Lax–Wendroff scheme in which an artificial dissipation was added to the equation to recover the destabilizing effects of the known anti-diffusion due to the first-order time discretization. The only unsatisfactory aspect of the method applied was a small amount of smoothing close to the sharp front tip of the interface. This feature was found to be consistent with time since the flux function and added dissipation vanish in both walls.

3.1. *Examples of typical qualitative behaviour*

Example computed HL displacements are shown in figure 4. The results at long times are not found to be particularly sensitive to the initial condition, which we have taken as a linear function of ξ: typically $h(\xi, T = 0) = \mp\xi \pm 0.5$ for HL and LH displacements, respectively. When we have wished to study the early-time evolution of the interface, we steepen the initial profile, e.g. in figure 4(*a*) the initial condition is $h(\xi, T = 0) = -\xi + 0.05$. Figures 4(*a*) and 4(*b*) plot the solution for $m = 1$, $\chi = 0$, (i.e. equal viscosities in a perfectly horizontal channel). In the early times, $T \in [0, 1]$

we observe that the interface develops quickly into a slumping profile; see figure 4(*a*). Over longer times, the solution consists of two segments: an advancing front of apparently constant shape moving at constant speed and a region at the top which is *stretched*, the top of the interface simply not moving. The longer time profiles of h may be conveniently plotted against ξ/T, in which variable the interface profiles collapse to a single similarity profile as $T \to \infty$ (figure 4*b*). To clarify interpretation of figures such as figure 4(*b*), the x-axis of the final similarity profile gives the speed of the interface at different heights: vertical lines correspond to segments of the interface that advance at steady speed.

Note that the first interface profile in figure 4(*b*), for $T = 1$, effectively shows $h(\xi, T)$ at $T = 1$, and in this we may observe that the top of the interface is *pinned* to the upper wall at the initial position $\xi = -0.5$. The convergence at the upper wall as $T \to \infty$ simply follows $\xi/T = -0.5/T$, and the interface itself does not move, as evidenced in figure 4(*a*) over shorter times. Thus, the apparent discrepancy between the last interface profile of figure 4(*a*) and the first interface profile of figure 4(*b*) is simply due to the different initial conditions.

This qualitative behaviour is similar for other parameters and indeed convergence to the 'final' similarity profile is relatively quick, occurring over an $O(1)$ time scale (in T). For our other results we present only the interface at $T = 10$, which is always very close to the final similarity profile. Figure 4(*c*) shows the final shape for three different values of viscosity ratio m and figure 4(*d*) shows the final shape for three different values of the inclination parameter χ. For larger m the height of the steadily moving front, say h_f, is smaller. This is intuitive, since increasing m corresponds to an increasingly less viscous fluid displacing a more viscous fluid. The interface above the steadily moving front also transitions from convex to concave curvature as m is increased, further emphasizing the extending finger. Similarly, for $\chi > 0$ the heavy fluid flows downhill through the lighter fluid and h_f is accordingly smaller in this configuration. The inset figures in figures 4(*c*) and 4(*d*) show the analogous LH displacements for the same parameters. The effects of m are identical with those for the HL displacement, (since m is the ratio of *in-situ* fluid viscosity to displacing fluid viscosity). The effect of varying χ is however reversed: $\chi > 0$ retards unsteady spreading for an LH displacement and $\chi < 0$ promotes unsteady spreading.

3.2. *Long-time behaviour*

We have seen in figure 4 that the interface tends to evolve on an $O(1)$ time scale into a shape that consists of two parts: (i) a front region that remains approximately constant but advances at steady speed; (ii) a stretched region, in which the interface is continually extended, as $t \to \infty$. For the HL displacement the steadily moving front occupies the lower part of the channel, and for the LH displacement the front advances along the upper wall. In place of computations, we would like to directly compute this long-time behaviour. In what follows below we focus for simplicity on the HL displacements.

We commence with the upper stretched region. If we denote the steady front height and speed by h_f and V_f, respectively, we observe that at long times the slope of the interface is approximately

$$\frac{\partial h}{\partial \xi} \sim -\frac{1 - h_f}{V_f T} \to 0, \text{ as } T \to \infty.$$

Therefore, as $T \to \infty$, we have that $b = \chi - \partial h/\partial \xi \to \chi$, and the interface motion in the stretched region is governed approximately by

$$\frac{\partial h}{\partial T} + \frac{\partial}{\partial \xi} q(h, \chi) = 0, \tag{3.1}$$

which is hyperbolic rather than parabolic. The interface in this region advances with speed $V_i(h)$ given by

$$V_i(h) = \frac{\partial q}{\partial h}(h, \chi).$$

Thus, the total area of fluid flowing behind the interface in the interval $[h_f, 1]$ at long times is

$$T \int_{h_f}^{1} V_i(h)\, \mathrm{d}h = T[1 - q(h_f, \chi)].$$

Furthermore, at the front height h_f the interface speed should equal the front velocity V_f, i.e.

$$\frac{\partial q}{\partial h}(h_f, \chi) = V_i(h_f) = V_f. \tag{3.2}$$

The total area of fluid behind the interface is T and since the area of fluid flowing behind the interface in the interval $[0, h_f]$ is approximately $TV_f h_f$, we have the following relationship:

$$Tq(h_f, \chi) = T - T[1 - q(h_f, \chi)] = TV_f h_f = Th_f \frac{\partial q}{\partial h}(h_f, \chi),$$

from which

$$q(h_f, \chi) = h_f \frac{\partial q}{\partial h}(h_f, \chi). \tag{3.3}$$

Equation (3.3) is an equation for the front height h_f. This is instantly recognizable as the same condition that must be satisfied in the case of a kinematic shock, in order to conserve mass. Therefore, note that the long time behaviour is that determined by the underlying hyperbolic conservation law.

An example of the use of the *equal areas rule* (3.3) to determine the front height is shown in figure 5(*a*). In figure 5(*b*) we plot h against ξ/T for $T = 1, \ldots, 9,\ 10$, showing that h_f does indeed represent the moving front, which has the same speed as indicated in figure 5(*a*). Although for most of the parameters we have considered, there is a single propagating front, some parameters result in a double front. Loosely speaking, for Newtonian fluids this appears to arise at more extreme parameter values when physical effects are somehow opposing one another. An example is shown in Figures 5(*c*) and 5(*d*). In this illustration, the competing effects are buoyancy, driven by the downhill slope which acts to spread the interface, and the viscosity ratio which acts to sharpen the front.

Figure 6(*a*) shows calculated front heights for HL and LH displacements for different values of χ and m. To interpret this figure for the LH displacement The front height h_f for LH displacement is defined as the distance from the top wall to the stretched part of the interface. We observe that higher viscosity ratios tend to have a lower front height, which simply means that in order to have a more efficient displacement, the displacing fluid should be more viscous in comparison to the displaced fluid. Increasing χ tends to reduce efficiency for the HL displacement but increase efficiency for the LH displacement. Via repeated computation of q for different (m, χ) we are able to delineate the regime in the (m, χ) plane in which

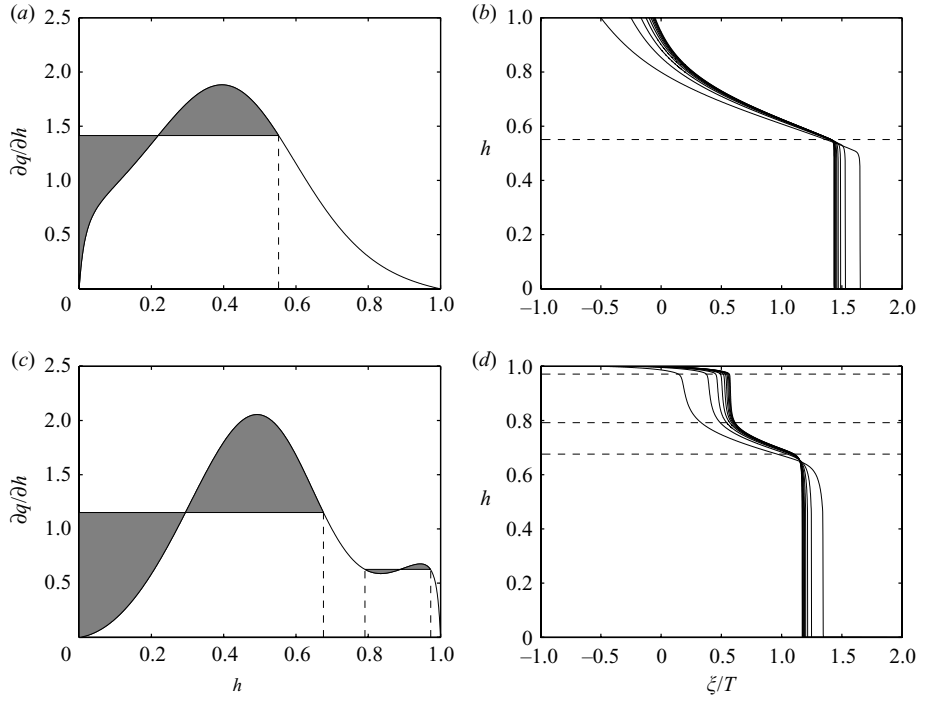

FIGURE 5. Use of the equal areas rule (3.3) in determining the front height: (*a*) a single front height, $\chi = 10, m = 8$; (*b*) h plotted against ξ/T for $T = 1, \ldots, 9, 10$, parameters $\chi = 10, m = 8$, broken horizontal line indicates the front height determined from (3.3); (*c*) two front heights, $\chi = 10, m = 0.08$; (*d*) h plotted against ξ/T for $T = 1, \ldots, 9, 10$, parameters $\chi = 10, m = 0.08$, broken horizontal lines indicate the front heights.

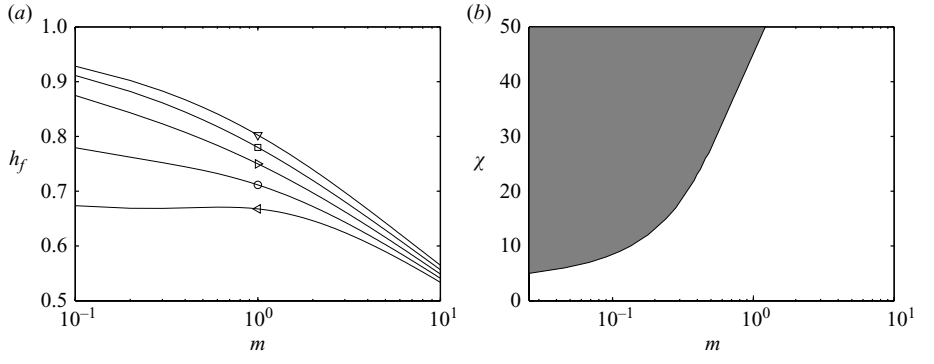

FIGURE 6. (*a*) Front heights for a Newtonian fluid HL displacement with $\chi = -10$ ($\triangledown$), $\chi = -5$ ($\square$), $\chi = 0$ ($\triangleright$), $\chi = 5$ ($\bigcirc$), $\chi = 10$ ($\triangleleft$). This figure also gives the front heights for a Newtonian fluid LH displacement with $\chi = 10$ ($\triangledown$), $\chi = 5$ ($\square$), $\chi = 0$ ($\triangleright$), $\chi = -5$ ($\bigcirc$), $\chi = -10$ ($\triangleleft$). For the LH displacement the front height is measured down from the top wall; (*b*) Parameter regime in the (m, χ) plane in which multiple fronts (shaded area). Elsewhere there is only a single front.

multiple fronts are found (figure 6*b*). Within the shaded region of figure 6(*b*), note that some parameter values give front speeds that are negative, i.e. there is a backflow driven by buoyancy.

Although the expression (3.3) for the front height is exactly the equation that would be solved for computing a kinematic shock for the hyperbolic conservation law, it is

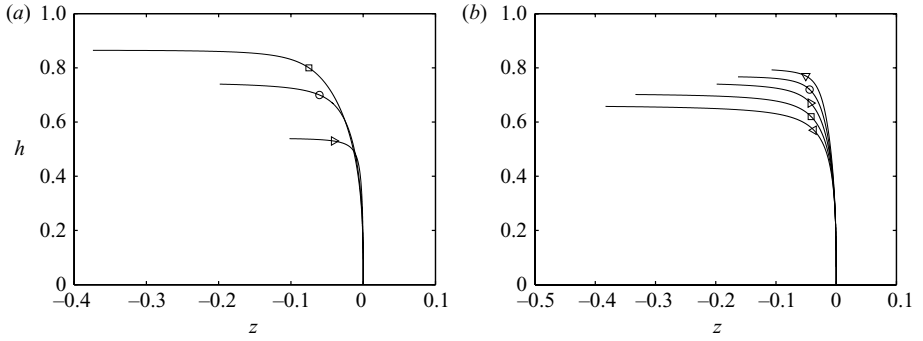

FIGURE 7. Examples of front shapes in the moving frame of reference for an HL displacement, computed from (3.4): (*a*) $\chi = 0$, $m = 0.1$ (□), $m = 1$ (○), $m = 10$ (▷); (*b*) $\chi = -10$ (▽), $\chi = -5$ (○), $\chi = 0$ (▷), $\chi = 5$ (□), $\chi = 10$ (◁). Compare with transient computations in Figures 4(*c*) and 4(*d*).

important to emphasize that the front is not a shock since diffusive effects are always present for $h \in (0, 1)$. Having determined h_f from (3.3) and then V_f from (3.2), we may shift to a moving frame of reference $z = \xi - V_f T$ and seek a steadily travelling solution to (2.23), which satisfies

$$\frac{\mathrm{d}}{\mathrm{d}z}\left[hV_f - q\left(h, \chi - \frac{\mathrm{d}h}{\mathrm{d}z}\right)\right] = 0, \quad \Rightarrow \quad hV_f - q\left(h, \chi - \frac{\mathrm{d}h}{\mathrm{d}z}\right) = 0. \tag{3.4}$$

Equation (3.4) must be solved numerically for $h \in (0, h_f)$. Example shapes are shown in figure 7. Figure 7(*a*) shows HL displacement front shapes for two Newtonian fluids for different values of viscosity ratio at $\chi = 0$. Figure 7(*b*) shows HL displacement front shapes for two Newtonian fluids for different values of χ at $m = 1$. These are the same parameters as for the transient displacements in Figures 4(*c*) and 4(*d*). Observe from (3.4) as $h \to h_f^-$ that, since h_f is determined from (3.3) and V_f from (3.2), we must have

$$q\left(h, \chi - \frac{\mathrm{d}h}{\mathrm{d}z}\right) \to q(h_f, \chi) \text{ as } h \to h_f^-,$$

which implies that $\mathrm{d}h/\mathrm{d}z \to 0$ as $h \to h_f^-$, as can be seen in figure 7. Evidently, as $T \to \infty$ the stretched region of the interface also aligns horizontally, so that the long-time solution is smooth at h_f.

3.3. *Flow reversal and short-time behaviour*

The model results presented so far have been derived under lubrication scaling assumptions, with the length scale determined by dominant buoyancy effects, compatible with the assumed stratification. Our study of the long-time behaviour has revealed only forward propagating fronts, which of course are more common since a positive flow rate is imposed. If the channel is horizontal then, as the front advances and the slope of the interface decreases, the driving force to oppose the mean flow also diminishes. Thus, we cannot expect flow reversal in a horizontal channel at long times.

On the other hand, with an inclined channel there is a constant buoyancy force that may either reinforce or oppose the mean flow. For example, with an HL displacement at fixed positive inclination, $\chi > 0$, buoyancy acts to push the lighter fluid against the mean flow direction. For sufficiently large χ and small viscosity ratio, we observe that

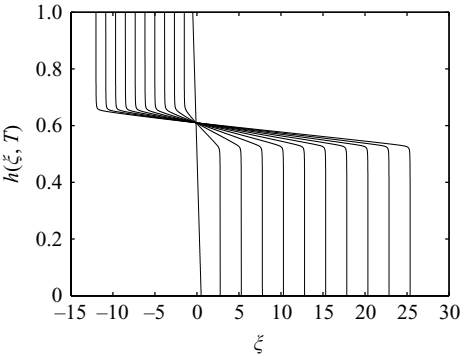

FIGURE 8. Profiles of $h(\xi, T)$ for $T = 0, 1, \ldots, 9, 10$, with parameters $\chi = 50$, $m = 0.1$, illustrating flow reversal.

the lighter fluid may be driven backwards against the flow, resulting in a sustained flow reversal. An example of this is shown in figure 8.

Flow reversal may also be observed in other situations. The most obvious of these is the case $T \ll 1$, since for short times large interface slopes may mean that gravitational spreading may dominate the imposed flow. Since our model is anyway an asymptotic reduction of the full equations in which T effectively represents a long-time relative to the advective time scale over the channel width, the limit $T \to 0$ is one in which the underlying assumptions of the model break down. Nevertheless, the problem for $T \ll 1$ is mathematically well defined and of physical interest.

To study this limit, we shift to the steadily moving frame of reference $z = \xi - T$, recall that $b = \chi - h_\xi$, and consider (2.23) for an HL displacement, which becomes

$$\frac{\partial h}{\partial T} + \frac{\partial}{\partial z}\left[q_A(h;m) + \left(\chi - \frac{\partial h}{\partial z}\right) q_B(h;m) - h\right] = 0, \tag{3.5}$$

where $q_A(h;m)$ and $q_B(h;m)$ represent the advective and buoyancy-driven components of the flux $q(h;b,m)$, which is defined by (2.29) for two Newtonian fluids, i.e. introducing $\eta = z/\sqrt{T}$ this becomes

$$\frac{1}{2}\eta\frac{\mathrm{d}h}{\mathrm{d}\eta} - \sqrt{T}\frac{\mathrm{d}}{\mathrm{d}\eta}\left(q_A - h + \chi q_B\right) + q_B\frac{\mathrm{d}^2h}{\mathrm{d}\eta^2} + \frac{\partial q_B}{\partial h}\left(\frac{\mathrm{d}h}{\mathrm{d}\eta}\right)^2 = 0. \tag{3.6}$$

Therefore, provided that $T \sim 0$ we may seek a similarity solution satisfying

$$\frac{1}{2}\eta\frac{\mathrm{d}h}{\mathrm{d}\eta} + q_B\frac{\mathrm{d}^2h}{\mathrm{d}\eta^2} + \frac{\partial q_B}{\partial h}\left(\frac{\mathrm{d}h}{\mathrm{d}\eta}\right)^2 = 0, \tag{3.7}$$

or in conservative form

$$\frac{1}{2}\eta\frac{\mathrm{d}h}{d\eta} = \frac{\mathrm{d}}{\mathrm{d}\eta}\left(-q_B\frac{\mathrm{d}h}{\mathrm{d}\eta}\right). \tag{3.8}$$

Since $q_B(h;m)$ vanishes at both $h = 0$ and $h = 1$, it is clear that there is some singular behaviour in $h(\eta)$ at these points. Thus, it is more comfortable to work with the function $\eta(h)$. The boundary conditions are $\eta(0) = \eta_0$ and $\eta(1) = \eta_1$, where η_0 and η_1 are unknown at this stage. Physically, we expect that $\eta_0 > 0$ and $\eta_1 < 0$ as the spreading of the interface is caused by gravitational slumping. A Taylor expansion reveals that $\eta(h) \sim \eta_0 + O(h^3)$ as $h \to 0$, with similar asymptotic behaviour as $h \to 1$,

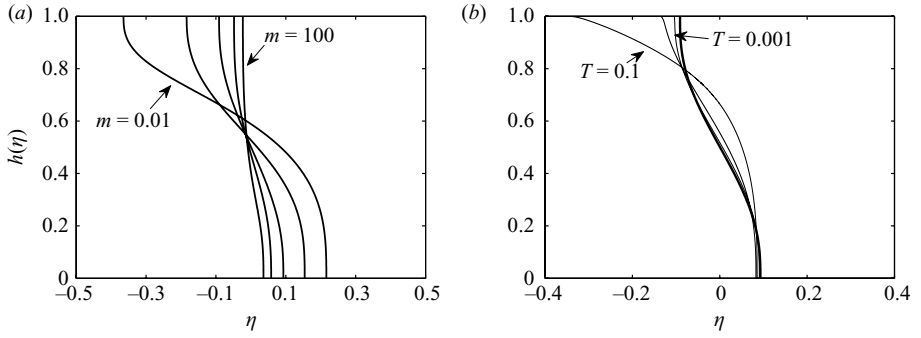

FIGURE 9. (*a*) the similarity solution $h(\eta)$ for $m = 0.01, 0.1, 1, 10, 100$; (*b*) comparison of the similarity solution with the numerical solution of (3.5) for $m = 1$, at $T = 0.001, 0.01, 0.1$.

i.e. $\eta'(h) \to 0$ quadratically at both ends of the interval. We integrate (3.8) as follows:

$$\frac{1}{2}\eta \mathrm{d}h = \mathrm{d}\left(-q_B \frac{\mathrm{d}h}{\mathrm{d}\eta}\right), \tag{3.9}$$

$$\int_0^h \frac{1}{2}\eta \mathrm{d}h = \int_0^h \mathrm{d}\left(-q_B \frac{\mathrm{d}h}{\mathrm{d}\eta}\right) = -q_B(h)\frac{\mathrm{d}h}{\mathrm{d}\eta} + q_B(0)\frac{\mathrm{d}h}{\mathrm{d}\eta} = -q_B(h)\frac{\mathrm{d}h}{\mathrm{d}\eta}, \tag{3.10}$$

(note $q_B(h) \to 0$ as $h \to 0$ with order h^3). Now taking $h \to 1$ and using the asymptotic behaviour $q_B(h) \sim (1-h)^3$, we have

$$\frac{1}{2}\int_0^1 \eta \, \mathrm{d}h = 0. \tag{3.11}$$

Let us now define $g(h)$ such that $\eta = g'$. Therefore,

$$g(h) - g(0) = \int_0^h \eta \cdot \mathrm{d}h, \tag{3.12}$$

and from (3.11), we see that $g(1) = g(0)$. For convenience, we set $g(0) = 0$ so that (3.10) may be written as

$$g'' \cdot g = -2q_B. \tag{3.13}$$

We use the initial condition $g(0) = 0$ and $g'(0) = \eta_0$. We then integrate forwards, with respect to h and iterate on η_0 via a shooting method to satisfy $g(1) = 0$.

This numerical procedure appears to work well. Figure 9(*a*) plots the similarity solutions $\eta(h)$ for various m. Note that the solution is not symmetric with respect to m. For the heavy–light displacement the heavy fluid viscosity is 1 and the light fluid viscosity is m. Buoyancy effects have no bias between the fluids, but the more viscous fluids evidently resist motion. Thus, we see that for large m the axial extension $\eta_0 - \eta_1$ is smaller than for small m. This effect might have been removed had we scaled viscosity with an appropriate mean value. A symmetrical shape is of course found at $m = 1$.

These solutions have been compared with the solution of PDE equation (3.5) as $T \sim 0$ and agree well for short times. An example is shown in figure 9(*b*) for the case $m = 1$. Mathematically, these solutions serve primarily to demonstrate that for short times, (e.g. after opening a gate valve in an experiment), buoyancy dominates and an exchange flow should occur, relative to the mean displacement. For smaller mean velocities the parameter $\delta \to 0$ and the dimensional time period over which buoyancy

dominates extends to infinity, ensuring compatibility with exchange flow studies, for which there is zero net flow rate and hence a flow reversal in each layer.

To explore this analogy further, let us fix $\beta = \pi/2$, in which case we may note that the similarity variable η is defined in terms of dimensional variables by

$$\eta = \frac{z}{T^{1/2}} = \frac{\hat{x} - \hat{U}_0\hat{t}}{\hat{t}^{1/2}} \sqrt{\frac{\hat{\mu}_1}{|\hat{\rho}_1 - \hat{\rho}_2|\hat{g}\hat{D}^3}}.$$

We may compare this with the analysis in Seon *et al.* (2007) for exchange flows in horizontal pipes, wherein diffusive similarity profiles are found for Newtonian fluids of the same viscosity. We may note that the scaling $|\hat{\rho}_1 - \hat{\rho}_2|\hat{g}\hat{D}^3/\hat{\mu}_1$ is the same as the $(V_v d)^{1/2}$ that scales the similarity variable $x/t^{1/2}$ in Seon *et al.* (2007) (see (27) and § VII.B in this paper). However, although this is the same viscous-buoyancy balance driving the diffusive spreading in both cases, here we have the additional criterion that $T^{1/2} \ll 1$, and we have seen numerically that the diffusive regime does not last for longer times. This criterion can be written dimensionally as

$$\frac{\hat{t}\hat{U}_0}{\hat{D}} \ll \frac{1}{\hat{U}_0} \frac{|\hat{\rho}_1 - \hat{\rho}_2|\hat{g}\hat{D}^2}{\hat{\mu}_1} = \frac{\hat{L}}{\hat{D}}.$$

The most simplistic interpretation therefore is that $\hat{t}\hat{U}_0 \ll \hat{L}$, i.e. the distance advected during the time considered must be much less than the characteristic slump length, (dimensionlessly, we require that $z \ll 1$). Alternatively the left-hand side is the ratio of advected distance to the channel width, whereas the quantity in the middle is the ratio of the viscous velocity scale to the advective velocity scale. Finally, observe that the short time diffusion is measured in a frame of reference moving with the mean velocity. The criterion $\hat{t}\hat{U}_0 \ll \hat{L}$ also means that the moving frame has not moved very far relative to the stationary frame in which the usual exchange flow analysis takes place.

4. Non-Newtonian fluids

We turn now to results for non-Newtonian fluids. Primarily, we shall be concerned with long-time results since the short-time behaviour does not yield simple analytical results in the form of similarity solutions. The reason for this becomes clear if we consider for example a Poiseuille flow of a power law fluid. The strain rate in the fluid is proportional to the pressure gradient to the $1/n$th power, and hence the areal flow rate also. In a two-layer flow of the type we have, the short-time behaviour is dominated by that part of $q(h, h_\xi)$ driven by the pressure gradient due to the slope of the interface. However, the flux in fluid layer k is proportional to $|h_\xi|^{1/n_k}$ and the two fluxes are coupled via the flow rate constraint. Thus, it is immediately obvious that there can be no single similarity variable unless the two fluids happen to have the same shear-thinning index. In this case the similarity variable is $\eta = z/t^{n/(n+1)}$. Although of mathematical interest, the practical interest is limited.

4.1. *Shear-thinning effects*

We commence by considering only shear-thinning effects $B_k = 0$, and shall also focus only on HL displacements. Figures 10(a) and 10(b) show the final similarity profiles of the interface for $m = 1$ and $\chi = 0$, i.e. the only effects are the relative values of the two power law indices. We observe that for fixed n_H the front height increases as n_L decreases. Conversely, for fixed n_L the front height decreases as n_H decreases.

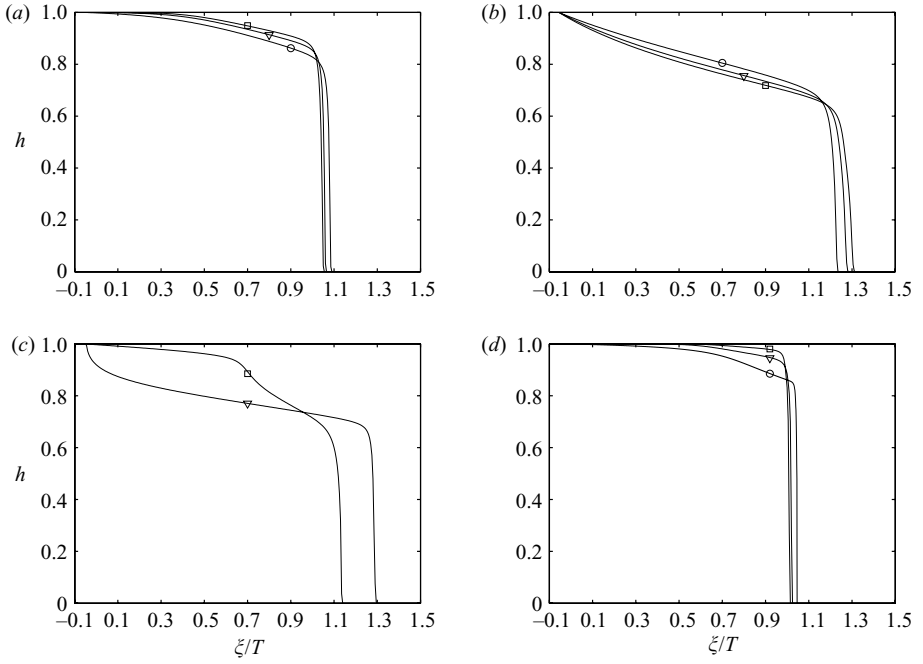

FIGURE 10. Examples of HL displacements for two power law fluids, $B_k = 0$, $\chi = 0$: (*a*) h for $m = 1, n_H = 1$: $n_L = 1/2$ (○), $n_L = 1/3$ (▽), $n_L = 1/4$ (□); (*b*) h for $m = 1, n_L = 1$: $n_H = 1/2$ (○), $n_H = 1/3$ (▽), $n_H = 1/4$ (□); (*c*) h for $n_H = 1/4, n_L = 1, m = 0.1$ (▽), $n_H = 1, n_L = 1/4, m = 10$ (□); (*d*) h for $m = 0.1, n_H = 1$: $n_L = 1$ (○), $n_L = 1/2$ (▽), $n_L = 1/4$ (□). All interfaces plotted at $T = 10$.

Both effects are essentially predictable, in that with all other parameters fixed (or neutralized in the case of inclination, $\chi = 0$), varying the power law indices makes one fluid progressively less or more viscous.

Less obvious effects are found when the 'bulk' viscosity of one fluid is for example large but has smaller power law index than the other fluid. For example, should $n_H = 1/4, n_L = 1, m = 0.1$ provide a better displacement than $n_H = 1, n_L = 1/4, m = 10$? Typically, in industrial settings one is unable to choose the rheological properties of the fluids. These displacements are shown in figure 10(*c*) and we see that in fact the latter case displaces better. Often shear-thinning behaviour can be brought about by the addition of a relatively small amount of a polymer additive. In cases when the displacement is anyway reasonable, due to a viscosity ratio $m < 1$, shear thinning effects can result in displacements that are close to 100 % efficient. An example of this are shown in figure 10(*d*), where for $m = 0.1$, $n_H = 1$ we show the effects of decreasing n_L. Note that as $n_L \to 0$, the light fluid effectively slips at the upper wall and we are able to have a steady travelling wave displacement.

The analysis of interface motion at long times is identical to that for the Newtonian fluid displacements of the previous section. The long-time behaviour can be analysed over a wide range of parameters by direct treatment of the flux function q. We present a range of parametric results below. Until now we have given only the front height h_f. However, in displacement experiments it is usually easier to estimate the front speed V_f from captured images, especially when the interface is diffuse. The front speed is calculated straightforwardly for Newtonian displacements, but for non-Newtonian fluids this is more laborious. A slightly different interpretation of the front

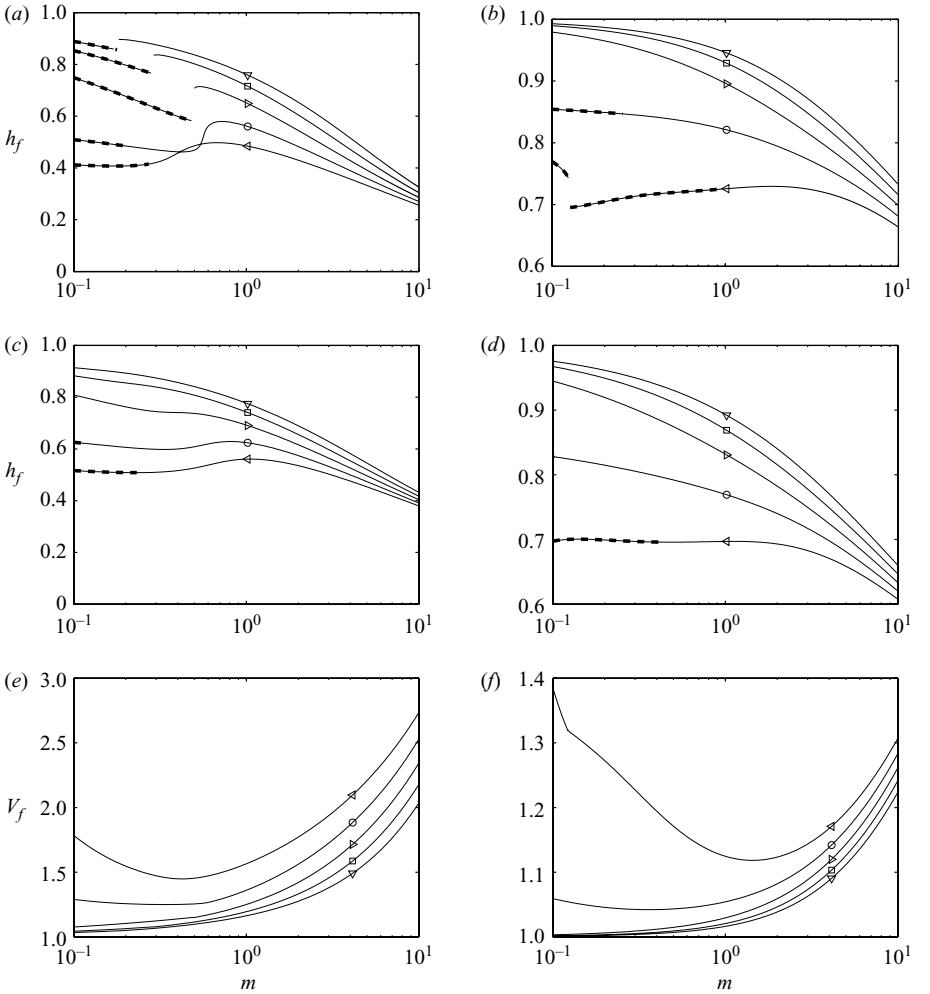

FIGURE 11. Front heights and velocities, plotted against m for an HL displacement of two power law fluids, $B_k = 0$; (*a*) h_f for $n_L = 1, n_H = 1/4$; (*b*) h_f for $n_H = 1, n_L = 1/4$; (*c*) h_f for $n_L = 1, n_H = 1/2$; (*d*) h_f for $n_H = 1, n_L = 1/2$; (*e*) V_f for $n_L = 1, n_H = 1/4$; (*f*) V_f for $n_H = 1, n_L = 1/4$. For all plots $\chi = -10$ ($\triangledown$), $\chi = -5$ ($\square$), $\chi = 0$ ($\triangleright$), $\chi = 5$ ($\circ$), $\chi = 10$ ($\triangleleft$), and the heavy broken line indicates multiple fronts.

speed is as an indicator of *displacement efficiency*. No single measure or definition is universal, e.g. for finite length ducts it is common to present quantities such as the volume fraction displaced after 1 volume of displacing fluid has been pumped, or alternatively after an infinite volume has been pumped. Here we define

$$\text{Displacement efficiency} = \frac{1}{V_f}. \tag{4.1}$$

At long times this approximates the area fraction behind the front that is displaced at time T. An alternative interpretation is as the *breakthrough time*, i.e. the time at which displaced fluid is first seen at unit length downstream.

Examples of variations in front height and speed, for different χ and m, as either n_H or n_L is reduced, are shown in figure 11. Essentially the displacement efficiency

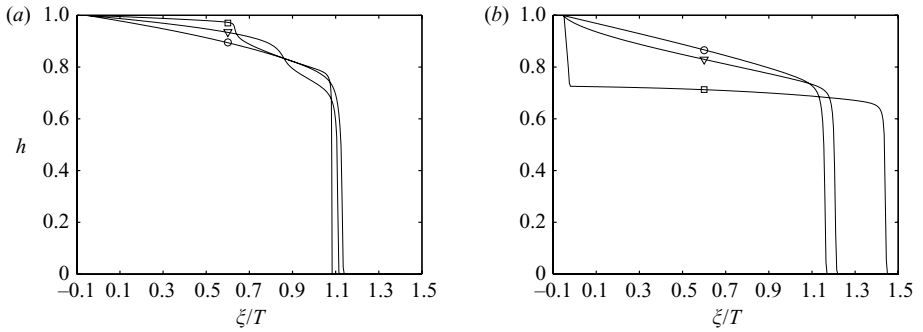

FIGURE 12. Profiles of h plotted against ξ/T at $T=10$: (*a*) $\chi=0, n_k=1, B_L=0, m=1$, $B_H=1$(○), $B_H=5$ (▽), $B_H=20$ (□); (*b*) $\chi=0, n_k=1, B_H=0, m=1$, $B_L=1$ (○), $B_L=5$ (▽), $B_L=20$ (□).

increases as the displacing fluid becomes less shear-thinning, as would be expected, and as the inclination increases. As with Newtonian displacements, for certain parameter ranges the long-time behaviour is characterized by two steady fronts, with the lower front moving faster. Parameters for which this happens are indicated in figure 11 by the heavy broken line. It can be observed that the transition from 1 front to 2 fronts can be either smooth or sudden. Later we illustrate in detail how these different transitions occur. For two Newtonian fluids the occurrence of multiple fronts is relatively easy to identify, as there are essentially only two effects that compete: viscosity and buoyancy (figure 6). However, for power law fluids we may have fluid combinations that are either more or less viscous than each other, for different shear rates, and these effects are then complemented with effects of different channel inclinations. Thus, the possible combinations of effects are vastly increased and it is hard to map out regions in parameter space where multiple fronts exist. Flow reversal occurs in HL displacements for large values of $\chi>0$ and for suitable viscosity ratios. For example, in figure 11(*b*) at small m for $\chi=10$, the heavy broken line indicates two moving fronts, but one front has negative speed (hence the decrease in efficiency). The jump in figure 11(*b*) (at small m for $\chi=10$) in fact indicates a transition from two fronts to three fronts: two moving forwards and one moving backwards!

4.2. *Yield stress effects*

We turn now to yield stress fluids and for simplicity we set $n_k=1$, i.e. these are Bingham fluids. Such fluids are in any case shear-thinning, due to the yield stress, but no additional power law behaviour is considered. We start by examining the effects of a single yield stress on a Newtonian displacement (for $m=1, \chi=0$) by increasing either B_H or B_L. Again only HL displacements are considered. Figure 12 shows the interfaces at $T=10$, plotted against ξ/T for each of these cases. It can be observed that increasing B_H improves the displacement due to the enhanced effective viscosity (figure 12*a*). Similarly, increasing B_L makes the displacement less efficient (figure 12*b*).

The new physical phenomena observed in figure 12(*b*) for larger B_L, is the possibility to have a static wall layer. Observe that for $B_L=20$ the interface at $T=10$ has not displaced the light fluid in the upper part of the channel. This will be attached to the upper wall in an HL displacement and to the lower wall in an LH displacement. This type of phenomena has been observed and studied before, both as part of a transient displacement flow and as a static situation (see, e.g. Allouche *et al.* 2000; Frigaard, Leimgruber & Scherzer 2003). We discuss static wall layer solutions further in § 4.2.1.

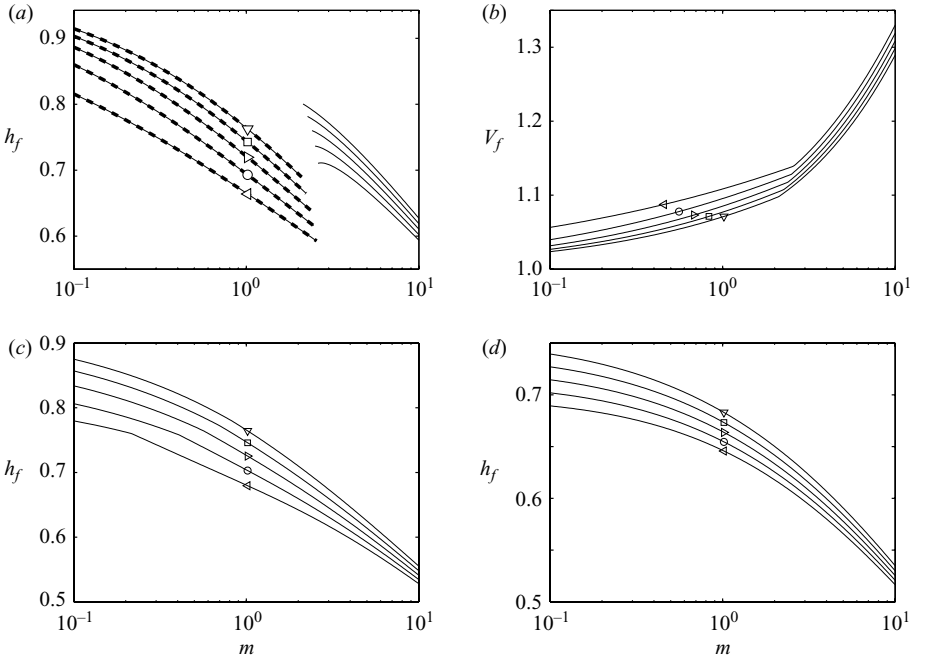

FIGURE 13. Front heights and velocities, plotted against m, $n_k = 0$; (a) HL displacement h_f versus m for $B_L = 0$, $B_H = 5$, (b) HL displacement V_f versus m for $B_L = 0$, $B_H = 5$, (c) HL displacement h_f versus m for $B_H = 0$, $B_L = 5$, (d) HL displacement h_f versus m for $B_H = 0$, $B_L = 20$. Parameters: $\chi = -10$ ($\triangledown$), $\chi = -5$ ($\square$), $\chi = 0$ ($\triangleright$), $\chi = 5$ ($\circ$), $\chi = 10$ ($\triangleleft$) for all plots. Broken heavy line indicates multiple fronts.

The long-time analysis of solutions is qualitatively similar to that discussed earlier. Examples showing the effects of χ and m on the front height and speed are shown in figure 13. General effects of varying m, χ and B_k are mostly in line with our physical intuition, i.e. effects that make the displacing fluid more viscous usually (but not always) improve the displacement. However, for parameter ranges where some ambiguity exists, this type of computation determines which effects dominate. We also observe the same range of different solution types as before when the parameters are varied, i.e. transitions from single to multiple fronts that may be smooth or sudden.

To clarify how transitions occur between single and multiple fronts (e.g. in figure 13 and similar figures previously), Figure 14 illustrates the two different type of transition, by showing $\partial q/\partial h(h, h_\xi = 0)$ at values of m just above and below the critical values at which transition occurs. In figures 14(a) and 14(b) we observe that the smooth transition typically corresponds to a change in the shape of $\partial q/\partial h(h, h_\xi = 0)$ from unimodal to bimodal (or vice versa). We have two fronts and as a process parameter is changed the slower front simply disappears. The sudden transition, illustrated in figures 14(c) and 14(d), is due to a change in the actual front height when switching between branches of a bimodal $\partial q/\partial h(h, h_\xi = 0)$. We have two fronts and as a process parameter is changed the slower front increases in speed, eventually overtaking the faster front, thus combining into one front. Note that there is no jump in the front speed (figure 13b). We have simply plotted the height of the fastest moving front, as this is the front that is most relevant for the displacement efficiency.

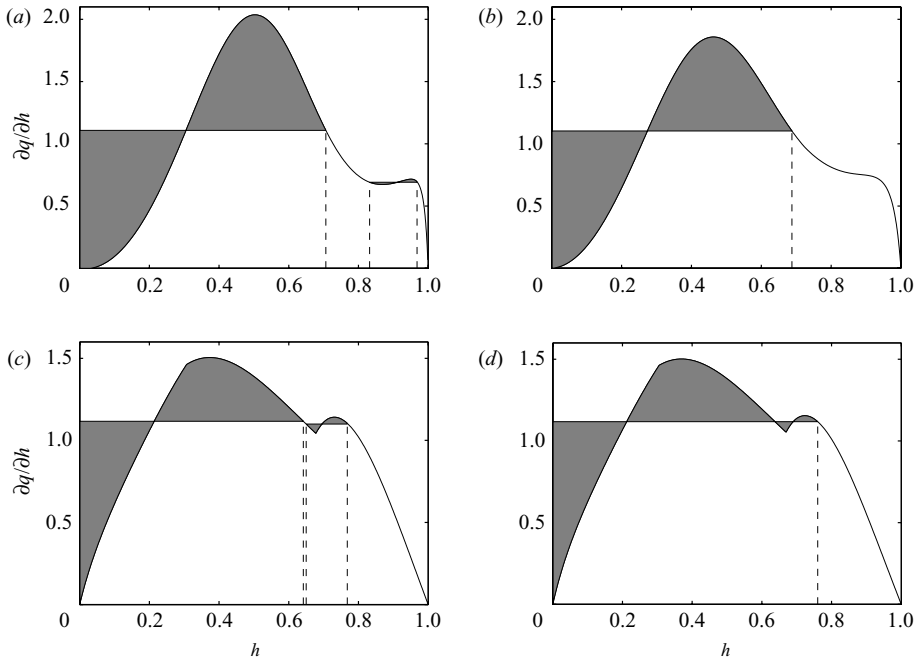

FIGURE 14. Plots of $\partial q/\partial h$ showing the front positions for parameters: $n_k = 1$: (*a*) $B_H = 1$, $B_L = 0$, $\chi = 10$, $m = 0.1$, multiple fronts; (*b*) $m = 0.2$, single front; (*c*) $\chi = 0$, $B_H = 5$, $B_L = 0$, $m = 2.3$, multiple fronts; (*d*) $\chi = 0$, $B_H = 5$, $B_L = 0$, $m = 2.4$, single front.

4.2.1. *The static wall layer*

The defining novel feature of a yield stress fluid displacement is the possibility for residual fluid to remain permanently in the channel, i.e. even asymptotically as $T \to \infty$ a fraction of fluid 2 may not be displaced. The origin of the static residual layer has a straightforward physical explanation. The lubrication displacement model that we study is based on an underlying parallel flow of two fluids. If the wall stress created by the displacing fluid, flowing at unit flow rate through the channel, does not exceed the yield stress of the displaced fluid, it follows that there could be a static residual layer on the wall. It can also be argued that there exists a uniquely defined maximal static layer thickness, either physically or mathematically (see Allouche *et al.* 2000; Frigaard *et al.* 2003).

On following a similar procedure to that of Allouche *et al.* (2000), we may show that the maximal residual wall layer thickness depends only on the following parameters (for an HL displacement):

$$n_H, \quad \tilde{B}_1 = \frac{B_H}{\kappa_H}, \quad \varphi_Y = \frac{B_H}{B_L}, \quad \varphi_b = \frac{\chi}{B_L}. \tag{4.2}$$

The parameter $\tilde{B}_1$ is a rescaled Bingham number, relevant to the displacing fluid; φ_Y is simply the yield stress ratio and φ_b measures the ratio of buoyancy stress due to the slope of the channel and the yield stress of the displaced fluid. The critical condition for the existence of any static wall layer is independent of the buoyancy ratio φ_Y.

Figure 15 shows the variation in maximum static wall layer Y_{static} with the parameters φ_Y and $1/\tilde{B}_1$ for three fixed values of the ratio φ_b. The shaded area

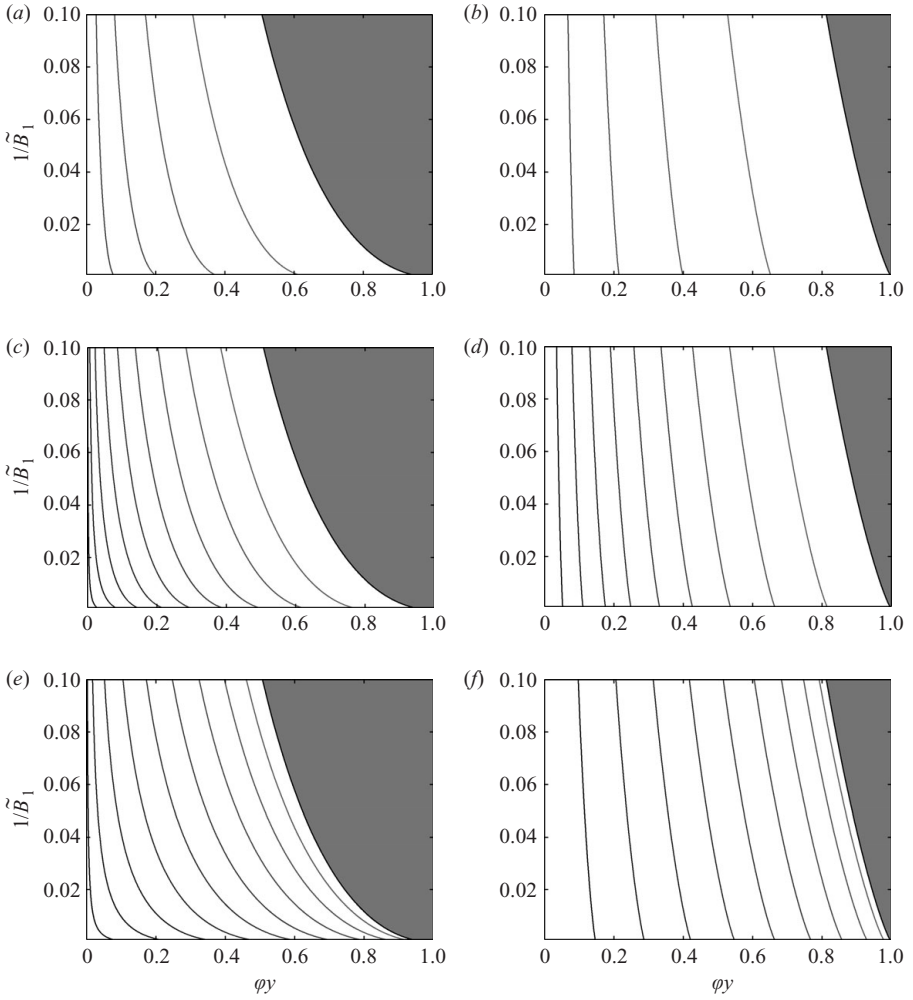

FIGURE 15. Maximal static wall layer thickness $Y_{static}(n_H, \tilde{B}_1, \varphi_Y, \varphi_b)$, with contours spaced at intervals $\Delta Y_{static} = 0.1$: (*a*) $\varphi_b = -2, n_H = 1$; (*b*) $\varphi_b = -2, n_H = 0.2$; (*c*) $\varphi_b = 0, n_H = 1$; (*d*) $\varphi_b = 0, n_H = 0.2$; (*e*) $\varphi_b = 2, n_H = 1$; (*f*) $\varphi_b = 2, n_H = 0.2$.

marks the limit where no static wall layers are possible. As n_H decreases, the contours become increasingly parallel to the vertical axis, which implies that the layer thickness is becoming independent of $\tilde{B}_1 = B_H/\kappa_H$. As φ_b increases from negative to positive the static layer thickness is increasing.

The limit $B_H \to 0$ must be treated separately. Straightforwardly, we find that Y_{static} depends on n_H, $\tilde{\chi} = \chi/\kappa_H$ and $\tilde{B}_2 = B_L/\kappa_H$. Figure 16 shows the variation in maximum static wall layer with the parameters $\tilde{\chi}$ and $\tilde{B}$ for four different fixed values of the power law index n_H. An interesting consequence of figure 16 is that for a small change in, e.g. yield stress, it appears that we may transition from having no static layer to having a finite static layer! An example illustration of this is given in figure 17. Although there is a discontinuity in the thickness of static layer, there is no discontinuity in the physical process, i.e. the layers of fluid that move do so very slowly as the static layer criterion is violated.

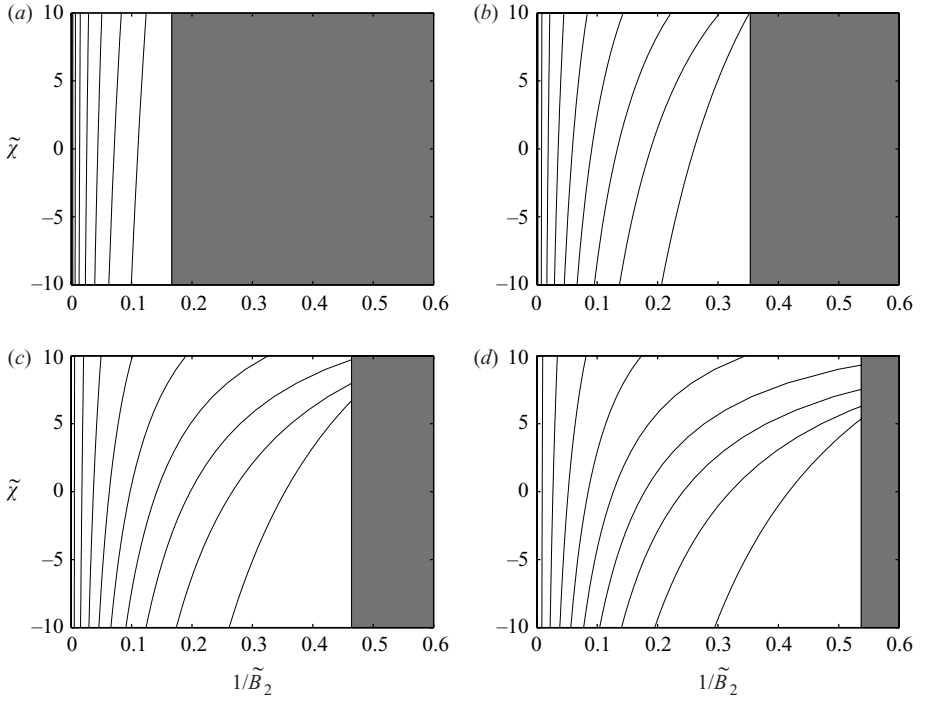

FIGURE 16. Maximal static wall layer $Y_{static} = 1 - h_{min}$ when a power-law fluid displaces a Herschel–Bulkley fluid, with contours spaced at intervals $\Delta Y_{static} = 0.1$: (*a*) $n_H = 1$; (*b*) $n_H = 1/2$; (*c*) $n_H = 1/3$; (*d*) $n_H = 1/4$.

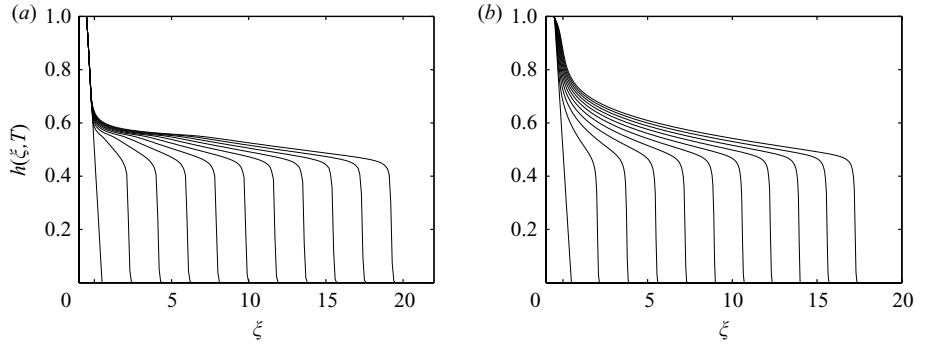

FIGURE 17. An example of sudden movement of static layer corresponding figure 16(*d*): (*a*) $h(\xi, T)$ for $T = 0, 1, \ldots, 9, 10$, parameters $\chi = 10, m = 1, n_H = 1/4, n_L = 1, B_1 = 0, B_2 = 2$; (*b*) $h(\xi, T)$ for $T = 0, 1, \ldots, 9, 10$, parameters $\chi = 10, m = 1, n_H = 1/4, n_L = 1, B_1 = 0, B_2 = 1$.

5. Discussion and conclusions

We have considered the viscous limit of a miscible displacement flow between parallel plates in the presence of strong density differences. The fluids considered are of generalized Newtonian type, and the principal tool used is a lubrication/thin-film approximation for long slumping flows. The principal contributions are as follows.

First, the semi-analytical solution for the flux functions, for yield stress and shear-thinning fluids (see Appendix A) has not been derived before. This solution allows one to consider this type of problem via fast computation. In the absence of such

a solution, to compute a solution requires numerical integration across the channel width in each fluid layer, coupled to iteration for the pressure gradients and stresses. In place we have simply to solve two coupled algebraic equations, both of which are monotone in their argument. This is a considerable step forwards.

We have analysed principally the long-time behaviour of displacement flows. Although these are termed 'long-time' solutions we have seen in most of our computed examples that the transients converge to something close to the long-time solutions over time intervals $T \sim O(1)$. These flows are characterized by intervals of interface that propagate at a constant speed (fronts), and other intervals in which the interface becomes progressively stretched. The front heights are determined by consideration of the associated hyperbolic problem and it appears that the long time solution converges to a similarity form $h(\xi/T)$.

A range of parametric results have been reported in which we explore variations in front heights and velocities with the model parameters. It is certainly fair to say that some of the results are predictable, e.g. more efficient displacements are generally found with a more viscous displacing fluid and some modest improvements can also be gained with slight positive inclination of the channel in the direction of the density difference. However, the value of the analysis really comes from quantifying the displacements, in terms of front heights and speeds, and in particular in helping to determine efficiency in cases where physical effects are ambiguous (figure 10*c*).

Probably the most impressive improvements in displacement efficiency arise when the displaced fluid is significantly shear-thinning, by comparison with the displacing fluid (figure 10*d*). Introduction of a yield stress can help displacements by making the displacing fluid more viscous, but if the displaced fluid has a yield stress it is very common to find completely static residual wall layers of displaced fluid. These are by-passed by the advancing front. Their thickness corresponds to the maximal static layer thickness and this can be computed directly, as we have done.

The key theoretical result is to establish that there can be no 100 % efficient displacements in this flow, regardless of rheological properties of the fluids (see Lemma 3 in § 2.4). A consequence of this is that we can focus in two directions:

(*a*) For the lubrication/thin film flows that we study, we may investigate which rheological properties give the most efficient displacements and try more generally to understand the qualitative behaviour of solutions to the lubrication/thin film model. This has been the focus of the present paper.

(*b*) We may target attention at situations in which the underlying model assumptions break down, e.g. due to flow instabilities developing or to other phenomena that are discounted *a priori* in this type of model. This is where our ongoing research is directed.

In the above context, there are a number of model assumptions that merit discussion. First, let us emphasize that in lubrication/thin-film models there is always an underlying assumption about the interface configuration, i.e. here we have assumed that the slumping configurations of figure 2 are found for HL and LH displacements. For isodensity displacements we typically have a symmetric finger-like front advancing in the channel centre and there is no effect of interface slope or channel inclination. However, for small density differences both effects are present and we may expect the symmetry to be broken, with the interface moving progressively towards this slumping configuration. There is no inherent difficulty in modelling asymmetric finger-like fronts within the thin-film framework. The transition between a slumping and finger-like displacement has not been studied, to our knowledge, and it is not clear to us how one would proceed to deduce the transition between interface configurations purely from

this type of model. An interesting paper in this context is Shariata *et al.* (2004), which illustrates that the resulting model systems can give rise to more complex behaviour than that considered here. In the experimental context, in the miscible fluid exchange flows of Seon *et al.* (2004, 2005, 2006, 2007), the interface is predominantly of the form of figure 2 when in the viscous regime, at near-horizontal inclinations. However, these experiments are conducted in a pipe and not a plane channel. Additionally, these experiments have no mean flow, so that no finger would be expected.

We note that although the result of Lemma 3 is established via a local analysis, as $h \sim 1$, and results essentially from the no-slip condition at the upper wall, the no-slip condition on its own does not imply that the interface can not propagate at steady speed along a wall. Indeed we have seen that this occurs at the lower wall at long times, for all parameters. More precisely, there is nothing mathematically present in the form of the lubrication model to prevent steady interface propagation. Indeed, an example of this occurs in Carrasco-Teja *et al.* (2008), where a Hele-Shaw displacement along a narrow concentric annulus is considered. Instead it is the algebraic form of q which distinguishes whether or not motion at the boundaries occur. Certainly, with slip at the upper wall we could achieve a steady displacement. This is the limiting case of $n_L \to 0$ for the shear-thinning study in figure 10(d). In Carrasco-Teja *et al.* (2008), symmetry conditions are imposed at the boundaries, which allows q to adopt a suitable algebraic form for steady-state propagation.

A related question concerns whether or not the scaling assumptions leading to the lubrication model may break down in the vicinity of the interface. In a strictly hyperbolic model (i.e. of the same algebraic form as we have, with $q = q(h, \chi)$), the moving front becomes a kinematic shock and the scaling assumptions break down. The kinematic and mass conservation equations are still valid, but the specification of the flux as a function only of the interface height becomes false. In our case however we have seen, e.g. in figure 7(b), that the interface is smooth and the frontal section of the interface has finite width in ξ. Thus, there is no reason for the scaling assumptions to become invalid.

A further interesting question concerns the stretched layer at the top of the channel (in an HL displacement). We note that the upper contact point of the interface does not move (unless we have backflow), and thus at long times we are left with a progressively thinning layer. We have seen that convergence to the long-time similarity profile typically occurs on a time scale $T \sim O(1)$. As the layer thins progressively, we may expect diffusive effects to become significant over a thickness $[T/(\delta Pe)]^{1/2}$ and could use the final similarity profile $h(\xi/T)$ to estimate evolution along the channel of the distance where diffusion is significant, i.e. effectively matching:

$$[T/(\delta\, Pe)]^{1/2} = 1 - h(\xi/T).$$

There are other interesting questions in this same direction, e.g. estimating dispersive characteristics of miscible displacement flows, in the spirit of Taylor dispersion. We leave these for future consideration.

This research has been carried out at the University of British Columbia, supported financially by NSERC and Schlumberger through CRD project 354716-07. T. Seon also acknowledges additional financial support from the Pacific Institute for the Mathematical Sciences through a post-doctoral fellowship. This support is gratefully acknowledged. We thank the reviewers for their suggestions which have helped improve the paper.

Appendix A. Computing the flux function $q(h, h_\xi)$

We address here the practicality of how to efficiently compute $q(h, h_\xi)$ for the non-Newtonian fluid types that we consider. Since $q(h, h_\xi)$ is defined in terms of $u = u(y, h, h_\xi)$, the first question is whether we may always find a velocity solution. The answer is yes, and we outline this later in § A.1.

For fixed h and $\partial h/\partial \xi$, (2.18) and (2.19) for an HL displacement are

$$\frac{\partial}{\partial y}\tau_{H,\xi y} = -f, \quad y \in (0, h), \tag{A 1}$$

$$\frac{\partial}{\partial y}\tau_{L,\xi y} = b - f, \quad y \in (h, 1), \tag{A 2}$$

where $f = -\partial P_0/\partial \xi$ and with $b = \chi - h_\xi$. Note that b physically represents the buoyancy forces that drive the flow, being divided into two components: χ, which represents the effects of the slope of the channel, and h_ξ, which represents the effects of the interface slope. Thus, the shear stresses are linear in y in each layer.

We denote the wall shear stresses in heavy and light fluid layers by τ_H & τ_L, respectively, which may be defined in terms of the pressure gradient $-f$ and interfacial stress τ_i as follows:

$$\tau_H = \tau_i + fh, \tag{A 3}$$

$$\tau_L = \tau_i + (1 - h)(b - f). \tag{A 4}$$

In terms of τ_i, τ_H and τ_L the shear stresses in each layer are

$$\tau_{H,\xi y}(y) = \tau_H \left(1 - \frac{y}{h}\right) + \tau_i \frac{y}{h}, \tag{A 5}$$

$$\tau_{L,\xi y}(y) = \tau_L \frac{h - y}{h - 1} + \tau_i \frac{1 - y}{1 - h}. \tag{A 6}$$

Using the constitutive laws of the two fluids, the velocity gradient $u'(y)$ is now defined at each point in the two fluid layers. We now integrate $u'(y)$ away from the walls at $y = 0$ and $y = 1$ (where the no-slip conditions are satisfied) towards the interface. Depending on the choices of τ_H, τ_L and τ_i, and the rheological parameters of each fluid, this leads to two interface velocities:

$$u_i(h^-) = \int_0^h u'(y; \tau_H, \tau_i)\, \mathrm{d}y, \tag{A 7}$$

$$u_i(h^+) = \int_1^h u'(y; \tau_L, \tau_i)\, \mathrm{d}y, \tag{A 8}$$

which need not be the same. For given wall stresses (τ_H, τ_L), we now iterate on τ_i, until

$$\Delta u_i(\tau_i) \equiv u_i(h^-) - u_i(h^+) = 0. \tag{A 9}$$

To make this procedure more clear, suppose that we have f fixed. For any given τ_i, the wall stresses (τ_H, τ_L) are defined by (A 3) and (A 4). As τ_i increases, both τ_H and τ_L increase. As the stress is linear in each layer and the constitutive laws are monotonic, this means that the velocity gradients in (A 7) and (A 8) increase with τ_i and therefore we see that $\Delta u_i(\tau_i)$ increases monotonically with τ_i. Therefore (A 9) always has a unique solution (this could in fact be stated more formally and proven). Thus, for given f we are able to determine all of τ_H, τ_L and τ_i by imposing continuity of the velocity at the interface and using (A 3) and (A 4). For Herschel–Bulkley fluids

we are in fact able to give an analytical expression for the interface velocities in terms of the wall and interfacial stresses:

$$u_i(h^-) = h\begin{cases} \dfrac{[H(|\tau_i|-B_H)(|\tau_i|-B_H)^{m_H+1} - H(|\tau_H|-B_H)(|\tau_H|-B_H)^{m_H+1}]}{\kappa_H^{m_H}(m_H+1)(\tau_i-\tau_H)} & \tau_i \neq \tau_H \\ \dfrac{\mathrm{sgn}(\tau_i)H(|\tau_i|-B_H)(|\tau_i|-B_H)^{m_H}}{\kappa_H^{m_H}(m_H+1)} & \tau_i = \tau_H \end{cases}, \tag{A 10}$$

$$u_i(h^+) = (h-1)\begin{cases} \dfrac{[H(|\tau_i|-B_L)(|\tau_i|-B_L)^{m_L+1} - H(|\tau_L|-B_L)(|\tau_L|-B_L)^{m_L+1}]}{\kappa_L^{m_L}(m_L+1)(\tau_i-\tau_L)} & \tau_i \neq \tau_L \\ \dfrac{\mathrm{sgn}(\tau_i)H(|\tau_i|-B_L)(|\tau_i|-B_L)^{m_L}}{\kappa_L^{m_L}(m_L+1)} & \tau_i = \tau_L \end{cases}, \tag{A 11}$$

where $H(x)$ is the usual Heavyside function. Note that $m_k = 1/n_k$. Thus, the iteration to find the solution of (A 9) involves simply a single monotone algebraic expression.

Having determined interfacial stress τ_i, we now integrate $u(y)$ across each layer to give the flow rates in each layer, which are thus determined as a function of f and b:

$$q_H = \begin{cases} hu_i(h^+) - \dfrac{h^2}{\kappa_H^{m_H}(\tau_i-\tau_H)^2}\left\{\mathrm{sgn}(\tau_H)H(|\tau_H|-B_H)\dfrac{(|\tau_H|-B_H)^{m_H+2}}{(m_H+1)(m_H+2)}\right. \\ \quad \left. + \mathrm{sgn}(\tau_i)H(|\tau_i|-B_H)(|\tau_i|-B_H)^{m_H+1}\left[\dfrac{B_H-\mathrm{sgn}(\tau_i)\tau_H}{m_H+1} + \dfrac{|\tau_i|-B_H}{m_H+2}\right]\right\} & \tau_i \neq \tau_H \\ hu_i(h^+) - \dfrac{h^2}{2\kappa_H^{m_H}}\mathrm{sgn}(\tau_i)H(|\tau_i|-B_H)(|\tau_i|-B_H)^{m_H} & \tau_i = \tau_H \end{cases}, \tag{A 12}$$

$$q_L = \begin{cases} (1-h)u_i(h^-) + \dfrac{(1-h)^2}{\kappa_L^{m_L}(\tau_i-\tau_L)^2}\left\{\mathrm{sgn}(\tau_L)H(|\tau_L|-B_L)\dfrac{(|\tau_L|-B_L)^{m_L+2}}{(m_L+1)(m_L+2)}\right. \\ \quad \left. + \mathrm{sgn}(\tau_i)H(|\tau_i|-B_L)(|\tau_i|-B_L)^{m_L+1}\left[\dfrac{B_L-\mathrm{sgn}(\tau_i)\tau_L}{m_L+1} + \dfrac{|\tau_i|-B_L}{m_L+2}\right]\right\} & \tau_i \neq \tau_L \\ (1-h)u_i(h^-) + \dfrac{(1-h)^2}{2\kappa_L^{m_L}}\mathrm{sgn}(\tau_i)H(|\tau_i|-B_L)(|\tau_i|-B_L)^{m_L} & \tau_i = \tau_L \end{cases}. \tag{A 13}$$

The sum of the two flow rates gives the total flow rate. As argued above, and also proven in § A.1, we can show that the total flow rate increases with f. Consequently we may use any flow rate constraint to find f, via iteration. The equation for the frictional pressure drop f is then

$$q_H + q_L = 1, \tag{A 14}$$

which is again a single monotone algebraic equation. Finally, we have the solution:

$$q(h, h_\xi) = q_H, \quad \frac{\partial P_0}{\partial \xi} = -f.$$

Computationally, the interfacial stress and modified pressure gradient are found via a nested iteration, i.e. for fixed f we find τ_i in an inner iteration and then find f in an outer iteration. The inner iteration for τ_i finds a zero of (A 9). On physical grounds we should expect that the interfacial stress lies somewhere between the wall stresses for each of the fluid phases. This allows us to prescribe upper and lower bounds for τ_i for the iteration. The iteration for f is based on solving the flow rate constraint (A 14). On physical grounds, we might expect the pressure gradient for the stratified flow to lie between the pressure gradients required to pump the same flow rate of either pure fluid. This is however not the case where there are extreme differences in rheology and a significant density difference. Thus, instead we determine initial bounds for f numerically.

A.1. *Existence of a velocity solution*

Following the steps in Frigaard, Leimgruber & Scherzer (2003), for any f and b, for fixed rheological constants and h we may write the problem for finding the velocity $u(y)$ as the following variational inequality:

$$\begin{aligned} &a(u, v-u) + j(v) - j(u) \geqslant f\,Q_H(v-u) + (f-b)Q_L(v-u), \\ &\quad u \in W_0^{1,1+n^*}(\Omega), \forall v \in W_0^{1,1+n^*}(\Omega), \end{aligned} \tag{A 15}$$

where

$$\begin{aligned} a(u, v) &= a_H(u, v) + a_L(u, v) \\ &= \kappa_H \int_0^h |u_y|^{n_H-1} u_y v_y \mathrm{d}y + \kappa_L \int_h^1 |u_y|^{n_L-1} u_y v_y \,\mathrm{d}y, \end{aligned} \tag{A 16}$$

$$j(v) = j_H(v) + j_L(v) = B_H \int_0^h |v_y| \,\mathrm{d}y + B_L \int_h^1 |v_y| \,\mathrm{d}y, \tag{A 17}$$

$$Q_H(v) = \int_0^h v \,\mathrm{d}y, \quad Q_L(v) = \int_h^1 v \,\mathrm{d}y, \tag{A 18}$$

where $n^* = \min\{n_H, n_L\}$ and $W_0^{1,1+n^*}(\Omega)$ is a Sobolev space (see Hirsch & Lacombe 1999) defined on $\Omega = [0, 1]$ containing functions that are zero at $y = 0, 1$, in the appropriate sense. Using standard theory from convex analysis (see, e.g. Ekeland & Temam 1976), this type of variational inequality has a unique solution u.

For given f we shall denote the solution by u_f. We now consider two solutions u_{f_1} and u_{f_2}, corresponding to $f_1 \neq f_2$. Treating u_{f_1} as a test function for u_{f_2} and vice versa, we insert into (A 15) and sum, to give

$$a(u_{f_1}, u_{f_2} - u_{f_1}) + a(u_{f_2}, u_{f_1} - u_{f_2}) \geqslant [f_1 - f_2][Q_H(u_{f_2} - u_{f_1}) + Q_L(u_{f_2} - u_{f_1})]. \tag{A 19}$$

Using the strict convexity of $a(\cdot, \cdot)$ (see, e.g. Ekeland & Temam 1976), it follows that

$$[f_2 - f_1][Q_H(u_{f_2} - u_{f_1}) + Q_L(u_{f_2} - u_{f_1})] \geqslant 0. \tag{A 20}$$

This inequality can be made strict provided that $u_f \neq 0$. Therefore, we see that the total flow rate $Q_H + Q_L$ increases monotonically with f, and strictly monotonically provided that $u_f \neq 0$ (which may happen for given yield stresses). Consequently, the criterion that

$$(Q_H + Q_L)(u_f) = 1, \tag{A 21}$$

is sufficient to uniquely determine f. The rate of increase of the individual Q_k with f can be estimated from the constitutive laws of the individual fluids. Monotonicity

of the flow rate with the applied pressure gradient is of course entirely intuitive from the physical perspective.

Appendix B. Monotonicity of q with respect to b

To demonstrate the monotonicity of q with respect to b, we use the variational method above. For fixed b (and rheological constants), we denote by (u_b, f_b) the solution (u, f) to (A 15) that satisfies the flow rate constraint (A 21). Since (A 21) is satisfied we may restrict the test space $W_0^{1,1+n^*}(\Omega)$ to the subspace $V \subset W_0^{1,1+n^*}(\Omega)$ such that (A 21) is satisfied for all $v \in V$. Consequently, (A 15) becomes

$$a(u, v-u) + j(v) - j(u) \geqslant -bQ_L(v-u), \quad u \in V, \forall v \in V. \tag{B 1}$$

We now consider two solutions u_{b_1} and u_{b_2}, to (B 1), corresponding to $b_1 \neq b_2$. Treating u_{b_1} as a test function for u_{b_2} and vice versa, we follow the same steps as in the above section for u_f to arrive at

$$[b_2 - b_1]Q_L(u_{b_2} - u_{b_1}) \leqslant 0. \tag{B 2}$$

Thus, Q_L decreases with b and since $q = 1 - Q_L$ we have that q increases with b.

REFERENCES

Allouche, M., Frigaard, I. A. & Sona, G. 2000 Static wall layers in the displacement of two visco-plastic fluids in a plane channel. *J. Fluid Mech.* **424**, 243–277.

Aris, R. 1956 On the dispersion of a solute in a fluid flowing through a tube. *Proc. R. Soc.* A **235**, 67–78.

Balmforth, N. J., Burbidge, A. S., Craster, R. V., Salzig, J. & Shen, A. 2000 Visco-plastic models of isothermal lava domes. *J. Fluid Mech.* **403**, 37–65.

Balmforth, N. J., Craster, R. V. & Sassi, R. 2002 Shallow viscoplastic flow on an inclined plane. *J. Fluid Mech.* **470**, 1–29.

Benjamin, T. J. 1968 Gravity currents and related phenomena. *J. Fluid. Mech.* **31**, 209–248.

Birman, V. K., Battandier, B. A., Meiburg, E. & Linden, P. F. 2007 Lock-exchange flows in sloping channels. *J. Fluid Mech.* **577**, 53–77.

Carrasco-Teja, M., Frigaard, I. A., Seymour, B. R. & Storey, S. 2008 Visco-plastic fluid displacements in horizontal narrow eccentric annuli: stratification and travelling wave solutions. *J. Fluid Mech.* **605**, 293–327.

Chen, C.-Y. & Meiburg, E. 1996 Miscible displacements in capillary tubes. Part 2. Numerical simulations. *J. Fluid Mech.* **326**, 57–90.

Coussot, P. 1999 Saffman–Taylor instability in yield-stress fluids. *J. Fluid Mech.* **380**, 363–376.

De Sousa, D. A., Soares, E. J., de Queiroz, R. S. & Thompson, R. L 2007 Numerical investigation on gas-displacement of a shear-thinning liquid and a visco-plastic material in capillary tubes. *J. Non-Newton. Fluid Mech.* **144** (2–3), 149–159.

Didden, N. & Maxworthy, T. 1982 The viscous spreading of plane and axisymmetric gravity currents. *J. Fluid Mech.* **121**, 27–42.

Dimakopoulos, Y. & Tsamopoulos, J. 2003 Transient displacement of a viscoplastic material by air in straight and suddenly constricted tubes. *J. Non-Newton. Fluid Mech.* **112** (1), 43–75.

Dimakopoulos, Y. & Tsamopoulos, J. 2007 Transient displacement of Newtonian and viscoplastic liquids by air in complex tubes. *J. Non-Newton. Fluid Mech.* **142** (1–3), 162–182.

Ekeland, I. & Temam, R. 1976 *Convex Analysis and Variational Problems*. North-Holland.

Frigaard, I. A., Leimgruber, S. & Scherzer, O. 2003 Variational methods and maximal residual wall layers. *J. Fluid Mech.* **483**, 37–65.

Frigaard, I. A., Scherzer, O. & Sona, G. 2001 Uniqueness and non-uniqueness in the steady displacement of two viscoplastic fluids. *ZAMM* **81** (2), 99–118.

Gabard, C. 2001 Etude de la stabilité de films liquides sur les parois d'une conduite verticale lors de l'ecoulement de fluides miscibles non-Newtoniens. PhD thesis, These de l'Universite Pierre et Marie Curie, Orsay, France.

Gabard, C. & Hulin, J.-P. 2003 Miscible displacements of non-Newtonian fluids in a vertical tube. *Eur. Phys. J.* E **11**, 231–241.

Griffiths, R. W. 2000 The dynamics of lava flows. *Annu. Rev. Fluid Mech.* **32**, 477–518.

Hirsch, F. & Lacombe, G. 1999 *Elements of Functional Analysis*. Springer.

Huppert, H. E. 1982 The propagation of two-dimensional and axisymmetric viscous gravity currents over a rigid horizontal surface. *J. Fluid Mech.* **121**, 43–58.

Joseph, D. D. & Renardy, Y. Y. 1993 Fundamentals of two-fluid dynamics. Part 2. *L*ubricated transport, drops and miscible liquids. In *Interdisciplinary Applied Mathematics Series*, vol. 4. Springer.

Kondic, L., Palffy-Muhoray, P. & Shelley, M. J. 1996 Models of non-newtonian Hele-Shaw flow. *Phys. Rev.* E **54** (5), 4536–4539.

Lajeunesse, E., Martin, J., Rakotomalala N. & Salin, D. 1997 Three-dimensional instability of miscible displacements in a Hele-Shaw cell. *Phys.* Rev. *Lett*. **79**, 5254–5257.

Lajeunesse, E., Martin, J., Rakotomalala, N. & Salin, D. 2001 The threshold of the instability in miscible displacements in a Hele-Shaw cell at high rates. *Phys. Rev. Lett*. **13** (3), 799–801.

Lajeunesse, E., Martin, J., Rakotomalala, N., Salin, D. & Yortsos, Y. 1999 Miscible displacement in a Hele-Shaw cell at high rates. *J. Fluid Mech.* **398**, 299–319.

Leal, G. 2007 *Advanced Transport Phenomena: Fluid Mechanics and Convective Transport Processes*. Cambridge University Press.

Lindner, A., Coussot, P. & Bonn, D. 2000 Viscous fingering in a yield stress fluid. *Phys. Rev. Lett*. **85**, 314–317.

Nelson, E. B. 1990 *Well Cementing*. Schlumberger Educational Services.

Petitjeans, P. & Maxworthy, T. 1996 Miscible displacements in capillary tubes. Part 1. Experiments. *J. Fluid Mech.* **326**, 37–56.

Rakotomalala, N., Salin, D. & Watzky, P. 1997 Miscible displacement between two parallel plates: BGK lattice gas simulations. *J. Fluid Mech.* **338**, 277–297.

Sader, J. E., Chan, D. Y. C. & Hughes, B. D. 1994 Non-Newtonian effects on immiscible viscous fingering in a radial Hele-Shaw cell. *Phys. Rev.* E **49** (1), 420–432.

Seon, T., Hulin, J.-P., Salin, D., Perrin, B. & Hinch, E. J. 2004 Buoyant mixing of miscible fluids in tilted tubes. *Phys. Fluids* **16** (12), L103–L106.

Seon, T., Hulin, J.-P., Salin, D., Perrin, B. & Hinch, E. J. 2005 Buoyancy driven miscible front dynamics in tilted tubes. *Phys. Fluids* **17** (3), 031702.

Seon, T., Hulin, J.-P., Salin, D., Perrin, B. & Hinch, E. J. 2006 Laser-induced fluorescence measurements of buoyancy driven mixing in tilted tubes. *Phys. Fluids* **18** (4), 041701.

Seon, T., Znaien, J., Salin, D., Hulin, J.-P., Hinch, E. J. & Perrin, B. 2007 Transient buoyancy-driven front dynamics in nearly horizontal tubes. *Phys. Fluids* **19** (12), 123603.

Shariata, M., Talon, M., Martin, J., Rakotomalala, N., Salin, D. & Yortsos, Y. C. 2004 Fluid displacement between two parallel plates: a non-empirical model displaying change of type from hyperbolic to elliptic equations. *J. Fluid. Mech.* **519**, 105–132.

Shin, J. O., Dalziel, S. B. & Linden, P. F. 2004 Gravity currents produced by lock exchange. *J. Fluid. Mech.* **521**, 1–34.

Taylor, G. I. 1953 Dispersion of soluble matter in a solvent flowing slowly through a tube. *Proc. R. Soc.* A **219**, 186–203.

Wilson, S. D. R. 1990 The Taylor–Saffman problem for a non-Newtonian liquid. *J. Fluid Mech.* **220**, 413–426.

Yang, Z. & Yortsos, Y. C. 1997 Asymptotic solutions of miscible displacements in geometries of large aspect ratio. *Phys. Fluids* **9** (2), 286–298.

Zhang, J. Y. & Frigaard, I. A. 2006 Dispersion effects in the miscible displacement of two fluids in a duct of large aspect ratio. *J. Fluid Mech.* **549** (1), 225–251.